OPTICAL MEMORY DEVELOPMENT

VOLUME III

The Membrane Light Valve Page Composer

BY

L. S. COSENTINO, E. M. NAGLE, AND W. C. STEWART

INTERIM REPORT

NOVEMBER 1972

PREPARED UNDER CONTRACT NAS8-26906

RCA LABORATORIES
PRINCETON, NEW JERSEY 08540

GEORGE C. MARSHALL SPACE FLIGHT CENTER
NATIONAL AERONAUTICS AND SPACE ADMINISTRATION
HUNTSVILLE, ALABAMA 35812

1. Report No.	2. Government Accession No.	3. Recipient's Catalog No.
Interim Report		

4. Title and Subtitle
OPTICAL MEMORY DEVELOPMENT
Volume III
The Membrane Light Valve Page Composer

5. Report Date
November 1972

6. Performing Organization Code

7. Author(s)
L. S. Cosentino, E. M. Nagle and W. C. Stewart

8. Performing Organization Report No.
PRRL-72-CR-55

9. Performing Organization Name and Address
RCA Laboratories
Princeton, New Jersey 08540

10. Work Unit No.

11. Contract or Grant No.
NAS8-26808

12. Sponsoring Agency Name and Address
George C. Marshall Space Flight Center
National Aeronautics and Space Administration
Huntsville, Alabama 35812

13. Type of Report and Period Covered
Interim Report
3/12/71 to 10/17/72

14. Sponsoring Agency Code

15. Supplementary Notes

16. Abstract
The feasibility of producing a page composer for optical memory systems using thin, deformable, membrane-mirror elements as light valves was investigated. The electromechanical and optical performances of such elements were determined both analytically and experimentally. It was found that fast switching (~10 μsec), high-contrast (10 or greater), fatigue-free operation over millions of cycles, and efficient utilization of input light could be obtained with membrane light valves. Several arrays of 64 elements were made on substrates with feedthroughs, allowing access to individual elements from the backside of the substrate. Single light valves on such arrays were successfully operated with the transistors designed and produced for selection and storage at each bit location. This simulated the operation of a prototype page composer with semiconductor chips beam-lead bonded to the back of the substrate. The fabrication details for making such a device were worked out during three practice cycles. All that remains is evaluation of the actual page composer when it is completed. While it has been shown that membrane elements make excellent light valves, it remains to be demonstrated that arrays of such valves can be produced without serious defects, and with enough uniformity to operate within practical tolerances. However, the remaining problems appear to be small ones which should yield to technological effort.

17. Key Words (Selected by Author(s))
Light valve
Page composer
Deformable membrane

18. Distribution Statement

19. Security Classif. (of this report)	20. Security Classif. (of this page)	21. No. of Pages	22. Price*
Unclassified	Unclassified	65	

*For sale by National Technical Information Service, Springfield, Virginia 22151.

FOREWORD

This interim report was prepared by RCA Laboratories, Princeton, New Jersey for the George C. Marshall Space Flight Center of the National Aeronautics and Space Administration, Huntsville, Alabama. It describes work done under Contract NAS8-26808 during the period from March 12, 1971 to October 17, 1972 in the Information Sciences Research Laboratory, Dr. Jan A. Rajchman, Staff Vice President and Director. The Project Supervisor was Mr. R. D. Lohman, Members of the Technical Staff who participated in the research reported herein are Mr. L.S. Cosentino, Mr. E. M. Nagle, and Dr. Wilbur C. Stewart. Messrs. V. Christiano, J. B. Harrison, and J.N. Hewitt aided in fabrication of the devices. The NASA Project Monitor was Mr. E. J. Reinbolt.

It should be noted that about 50% of the effort described in this report was supported by RCA Laboratories funds under its parallel research program and the remaining 50% was supported by contract funds.

TABLE OF CONTENTS

LIST OF ILLUSTRATIONS

LIST OF ILLUSTRATIONS (Continued)

LIST OF ILLUSTRATIONS (Continued)

THE MEMBRANE LIGHT VALVE PAGE COMPOSER

by

L. S. Cosentino, E. M. Nagle, and W. C. Stewart
RCA Laboratories
Princeton, New Jersey 08540

SUMMARY

The feasibility of producing a page composer for optical-memory systems using thin, deformable, membrane-mirror elements as light valves was investigated. The electromechanical and optical performances of such elements were determined both analytically and experimentally. It was found that fast switching (~10 μsec), high-contrast (10 or greater), fatigue-free operation over millions of cycles, and efficient utilization of input light could be obtained with membrane light valves. Several arrays of 64 elements were made on substrates with feedthroughs, allowing access to individual elements from the backside of the substrate. Single light valves on such arrays were successfully operated with the transistors designed and produced for selection and storage at each bit location. This simulated the operation of a prototype page composer with semiconductor chips beam-lead bonded to the back of the substrate. The fabrication details for making such a device were worked out during three practice cycles. All that remains is evaluation of the actual page composer when it is completed. While it has been shown that membrane elements make excellent light valves, it remains to be demonstrated that arrays of such valves can be produced without serious defects, and with enough uniformity to operate within practical tolerances. However, the remaining problems appear to be small ones which should yield to technological effort.

1. INTRODUCTION

The goal of this research was to determine the feasibility of producing a page composer for optical-memory systems using thin, deformable, membrane-mirror elements as light valves. Selection and memory in an 8×8 array was to be accomplished using semiconductor circuitry on the back-side of a substrate. Electrical connections to the element-drive electrodes were to be made via conductive feedthroughs in the substrate extending from the front surface to the back one. The device to be delivered to NASA was to demonstrate that fast, large-aperture, high-contrast, non fatiguing operation was possible with efficient reflection of incident laser light.

Earlier efforts with membrane light valves included the membrane light modulator (MLM) of Preston (ref. 1) which was utilized in an optical computer, the photo-activated MLM of Reizman (ref. 2) which was used as an image converter, and the schlieren light valve (SLV) of Van Raalte (ref. 3) which was used in a television projection system. This work extends the results in utilizing membrane light valves as elements of a page composer for an optical-memory system.

The basic membrane light-valve (MLV) geometries are described first, after which, electro-mechanical and optical responses of the light valves are analyzed. Fabrication and processing are treated next. The 8×8 delivery device is then described and discussed. Finally, experimental data for all of the devices are presented followed by discussions of the results and conclusions.

II. MEMBRANE LIGHT VALVE GEOMETRIES

All of the membrane light valves consist of a thin, metal film suspended over a support structure which defines the basic shape of the elements. A counter-electrode must be provided beneath the element, to which voltage is applied to activate the light valve with the membrane grounded. The electrostatic attraction between the membrane and the drive electrode causes the metal film to deform from its initially flat state. In the process, the reflection of light from the film surface changes from specular to scattering. An aperture can be appropriately placed in the optical system, such that, the specularly reflected light passes through it while most of the light reflected in a non-planar fashion does not get through the aperture. Thus, optical contrast can be achieved at a detector located after the aperture.

A line element is shown in Fig. 1(a) which is grossly exaggerated in the vertical dimension for clarity. A typical line element might have a separation between membrane and electrode of a few micrometers, an element width between supports of 0.25 mm, a membrane thickness of about 0.5 μm, and support structure widths which are 5-10% of the element width. The line element has a line electrode beneath it running the entire length of the element.

Another membrane light-valve geometry is shown in Fig. 1(b). This element has cylindrical holes in a support structure which defines circular elements in the membrane which is eventually suspended on the supports. The electrode (not shown) beneath the element may also be circular, or it may be of another shape if a portion of it is opposite the active area of the membrane.

Other geometries are also possible for membrane light valves. Figure 1(c) shows a support structure which defines square elements when a membrane is suspended on it. An individual electrode (not shown) can be located beneath each square to activate one element, or one large electrode can be located beneath several elements and simultaneously activate the group of elements. For instance, an electrode could be located to activate a 3 × 3 group of elements simultaneously as a single light valve. With such a multiple-element light valve, redundancy is obtained so that perfection in the membrane is not required. Another advantage is that a large light valve could be built up from smaller elements which might make fabrication simpler in some cases.

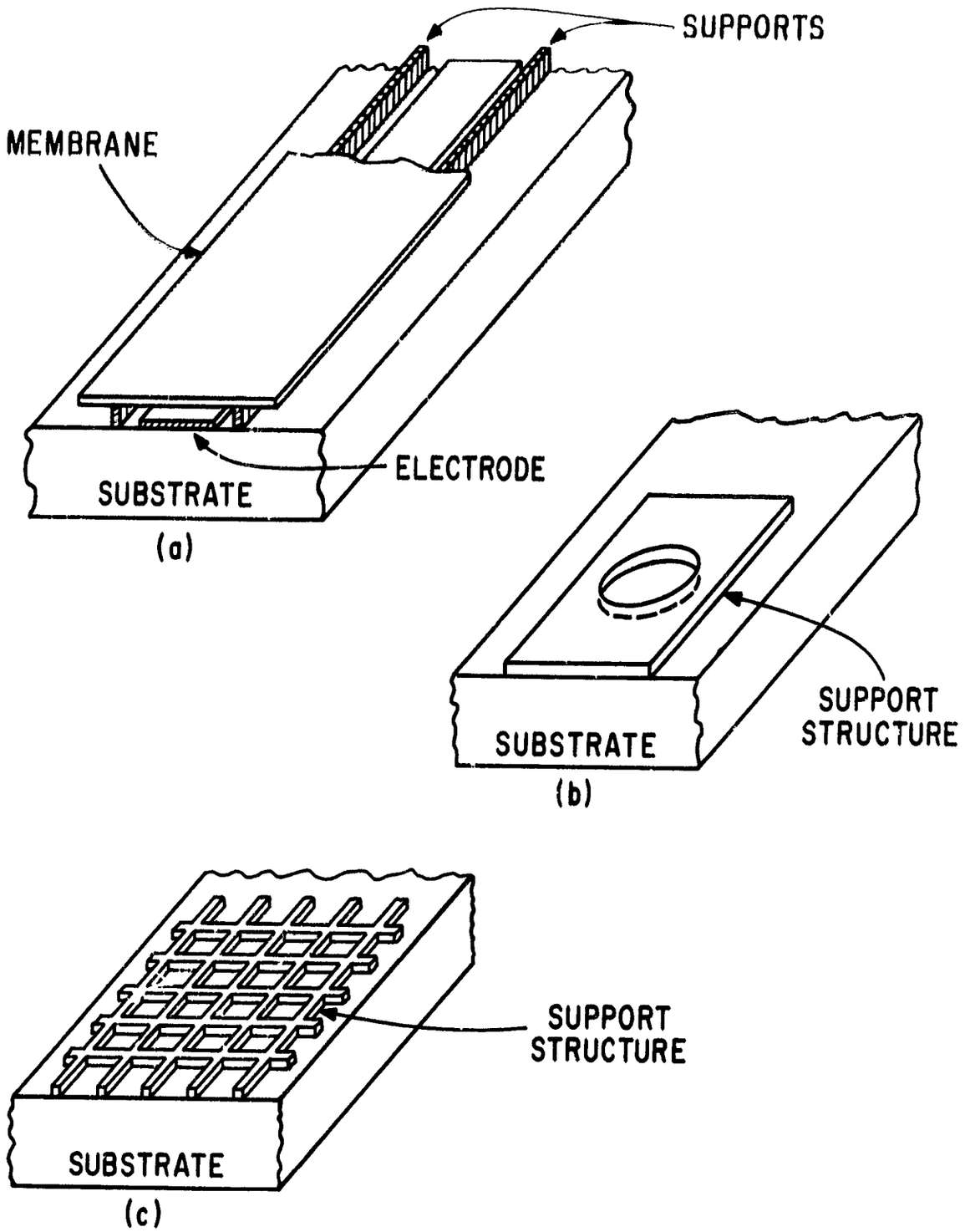

Figure 1. Membrane light-valve geometries.
(a) Line element.
(b) Circular cylindrical element (membrane and electrode not shown).
(c) Square element (membrane and electrode not shown).

III. ELECTROMECHANICAL OPERATION

When voltage is applied between an electrode and the membrane of a line element, such as the one shown schematically in Fig. 2(a), electrostatic attractive forces act to move the membrane towards the electrode until elastic restoring forces in the film are sufficient to prevent further deformation. The nature of the deformation can be determined with the aid of a free-body diagram of a section of the deformed membrane, with the sum of the forces equated to zero since the body is in equilibrium. When this is done, the resulting equation is

$$F = T_0 \frac{d^2 z}{ds^2} \tag{1}$$

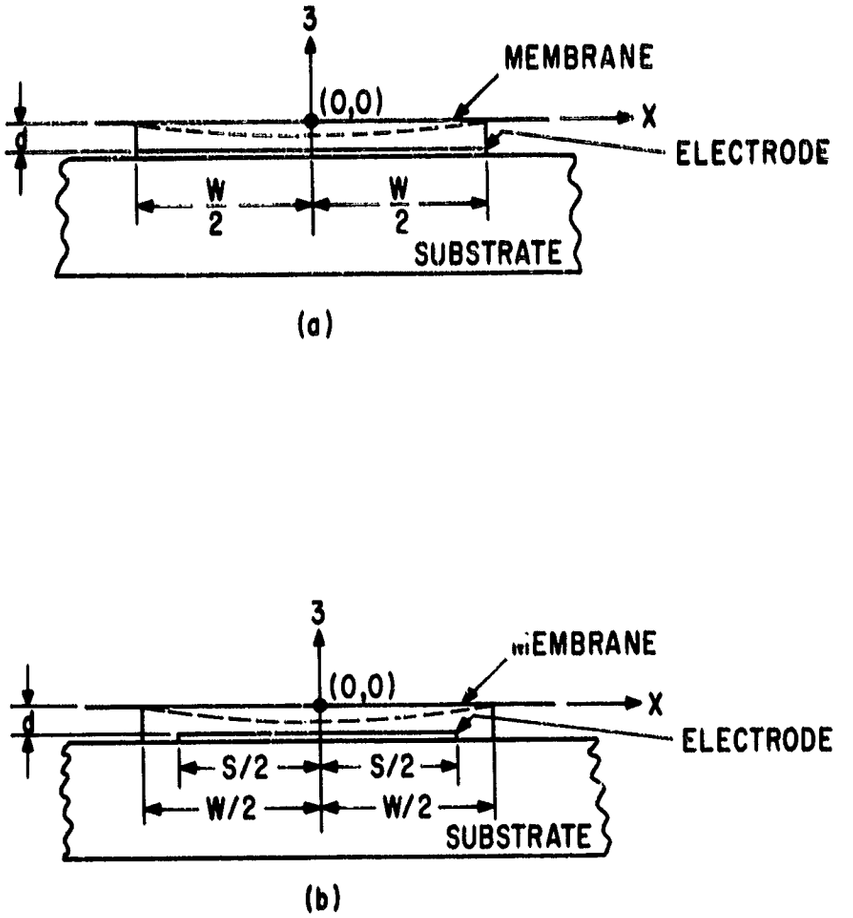

Figure 2. Line element with symbols used in calculation of deflection.
(a) Electrode extends over the full width of the element.
(b) Electrode is smaller than the element width.

where F is the electrostatic force per unit area, and T_0 is the film tension at the center of the element. Assuming an ideal parallel-plate capacitor, such as the one formed by the electrode and membrane if the deflection is negligible compared to the separation of the conductors, then

$$F = \epsilon V^2/2d^2 \tag{2}$$

where ϵ is the dielectric constant of the medium, V is the applied voltage, and d is the membrane to-electrode separation.

Therefore

$$T_0 \frac{d^2 z}{dx^2} = \frac{\epsilon V^2}{2d^2} \tag{3}$$

Solution of this equation with the appropriate boundary conditions gives the form of the deformation as

$$z = \frac{\epsilon V^2 W^2}{16 T_0 d^2} \left(\frac{4x^2}{W^2} - 1 \right) \tag{4}$$

which is seen to be parabolic. The maximum deflection which occurs at x = 0 is given by

$$z_0 = - \frac{\epsilon V^2 W^2}{16 T_0 d^2} \tag{5}$$

The foregoing assumed that the electrode extended beneath the entire width of the element. When this is not the case as in Fig. 2(b), a similar analysis results in

$$z = \frac{\epsilon V^2}{4 T_0 d^2} \left(x^2 + \frac{S^2}{4} - \frac{SW}{2} \right) \quad \text{for} \quad \frac{S}{2} \geq x \geq 0 \tag{6}$$

and

$$z = \frac{\epsilon V^2}{4 T_0 d^2} \left(\frac{S}{2} - x \right) \quad \text{for} \quad \frac{W}{2} \geq x \geq \frac{S}{2} \tag{7}$$

which describe a parabolic deformation region where the membrane is over the electrode and straight line segments connecting the ends of that region to the supports. The deformation at the center is somewhat reduced with narrow electrodes. If an electrode covered only half of the element width ($S = \frac{W}{2}$), z_0 would be three-quarters of the central deformation with a full width electrode (S = W).

The above analysis is valid whether the film tension (T_0) at the center of the deformed element was built into the film at the time of deposition, whether it results from elongation of the film, or even if it is a combination of these two tensions. For the case in which T_0 is a constant

not substantially affected by the stretching of the film, the derived equations are complete. If on the other hand, T_o arises only because of elongation with the tension in the undeformed state being equal to zero, the above equations are still valid but T_o is determined by other factors, such as the mechanical properties of the film and the amount of elongation of the film.

Young's modulus (E) is defined as the ratio of stress (σ) to strain (ϵ). Since in the thin film $\sigma = T_o/t$, where t is the film thickness, and $\epsilon = \frac{\Delta W}{W}$, then

$$T_o = \left(\frac{\Delta W}{W}\right) Et \tag{8}$$

For a curved line such as the deformed film of Fig. 2(a),

$$\Delta W = \int_{-W/2}^{W/2} \left(\frac{ds}{dx}\right) dx - W = 2 \int_{0}^{W/2} \sqrt{\left(\frac{dz}{dx}\right)^2 + 1}\ dx - W$$

where ds is the differential distance along the curved line. Since $\frac{dz}{dx} << 1$ for all practical cases,

$$\sqrt{\left(\frac{dz}{dx}\right)^2 + 1} \approx 1 + \frac{1}{2}\left(\frac{dz}{dx}\right)^2$$

and

$$\Delta W \simeq 2 \int_{0}^{W/2} \left[1 + \frac{1}{2}\left(\frac{dz}{dx}\right)^2\right] dx - W = \int_{0}^{W/2} \left(\frac{dz}{dx}\right)^2 dx$$

From Eq. (4),

$$z = \frac{\epsilon V^2 W^2}{16 T_o d^2}\left(\frac{4x^2}{W^2} - 1\right)$$

so that

$$\left(\frac{dz}{dx}\right)^2 = \frac{\epsilon^2 V^4}{4 T_o{}^2 d^4}\ x^2$$

After substitution and integration

$$\Delta W = \frac{\epsilon^2 V^4 W^3}{96 T_o{}^2 d^4}$$

and

$$\frac{\Delta W}{W} = \frac{\epsilon^2 V^4 W^2}{96 T_o^2 d^4} \tag{9}$$

Substitution in Eq. (8) yields

$$T_o = \left(\frac{\epsilon^2 V^4 W^2 \, Et}{96 \, d^4} \right)^{1/3} \tag{10}$$

and since from Eq. (5)

$$z_o = - \frac{\epsilon V^2 W^2}{16 T_o d^2}$$

Substitution of the value for T_o of Eq. (10) gives

$$z_o = 0.287 \left(\frac{\epsilon V^2 W^4}{d^2 Et} \right)^{1/3} \tag{11}$$

with

$$z = z_o \left(1 - \frac{4x^2}{W^2} \right) \quad \text{as before.}$$

Note that for a given sample Eq. (11) shows that

$$z_o \propto V^{2/3} \qquad \text{for the case of tension caused by elongation only}$$

while Eq. (5) shows

$$z_o \propto V^2 \qquad \text{for the case of a constant built-in tension.}$$

The change in tension along the membrane has been assumed to be negligible in all of the previous analysis so that T_o was not a function of x. This can be justified by a simple calculation to determine the tension at one of the supports . Since

$$T(x) = - T_o \frac{ds}{dx} = - T_o \sqrt{1 + \left(\frac{dz}{dx} \right)^2}$$

and from Eq. (4)

$$z = \frac{\epsilon V^2 W^2}{16 T_o d^2} \left(\frac{4x^2}{W^2} - 1 \right) = - z_o \left(\frac{4x^2}{W^2} - 1 \right)$$

then

$$\left(\frac{dz}{dx}\right)^2 = 64\,\frac{z_o^2\,x^2}{W^4}$$

and

$$T\left(\frac{W}{2}\right) = -T_o\sqrt{1+\frac{16\,z_o^2}{W^2}}$$

Since z_o is typically about 1 μm and W about 250 μm,

$$T\left(\frac{W}{2}\right) \approx -T_o\left[1+\frac{1}{2}\,\frac{16}{(250)^2}\right] = -T_o\left(1+\frac{8}{62{,}500}\right) \approx -T_o\,(1.00013)$$

and

$$T\left(\frac{W}{2}\right) \approx -T_o$$

Therefore the tension is essentially constant and equal to T_o all along the membrane.

It is also of interest to calculate the incremental strain of the membrane for a typical deformation of 1 μm.

From Eq. (9)

$$\frac{\Delta W}{W} = \frac{\epsilon^2 V^4 W^2}{96\,T_o^2\,d^4} = 2.67\left(\frac{z_o}{W}\right)^2$$

Again letting W = 250 μm,

$$\frac{\Delta W}{W} = 0.43 \times 10^{-4} = 0.0043\%$$

This strain is quite small and well below the limit of elastic deformation which, for most metals, is is a strain of about 1%.

The dynamic response of a membrane line element is obtained by using Newton's Law, $F = ma = m\frac{d^2z}{dt^2}$, and equating this force to the elastic restoring force equal to $T_o\,\frac{d^2z}{dx^2}$. The resulting wave equation, with appropriate boundary conditions applied, has a solution which gives a vibration frequency of

$$f = \frac{n}{2W}\sqrt{\frac{T_o}{\delta t}} \qquad n = 1,2.3, \ldots \tag{12}$$

and

$$f_1 = \frac{1}{2W}\sqrt{\frac{T_o}{\delta t}} \tag{13}$$

is the fundamental mode. In these formulas, δ is the density of the membrane material, t is the thickness of the membrane, and T_o is assumed to be constant and unaffected by the motion. Also the formulas apply only to vacuum. In air there is mechanical damping caused by the gas molecules below the membrane, which resist deformation that tries to compress the volume of air. More will be said of this later.

Similar analyses can be performed for the other geometries of membrane elements. For the case of the circular element, the corresponding equations of deflection are

$$z = \frac{\epsilon V^2}{8 T_o d^2} \left(r^2 - \frac{D^2}{4} \right) \tag{14}$$

and

$$z_o = - \frac{\epsilon V^2 D^2}{32 T_o d^2} \tag{15}$$

where D is the diameter of the element. Note that the central deflection is about one-half that of a line element with width D for the equivalent conditions of tension, voltage, separation, etc.

The resonant frequency equation for the circular membrane is

$$f = \frac{p}{\pi D} \sqrt{\frac{T_o}{\delta t}} \tag{16}$$

where p equals the values at which the zero order Bessel function of the first kind $J_o(p)$ equals zero ($p_1 = 2.40$, $p_2 = 5.53$, $p_3 = 8.65$ etc.).

The fundametal mode is therefore given by

$$f_1 = \frac{0.764}{D} \sqrt{\frac{T_o}{\delta t}} \tag{17}$$

For the case of a square element, the corresponding deflection equation as derived from reference 4 is

$$z = - \frac{2 W^2 \epsilon V^2}{\pi^3 T_o d^2} \sum_{n = 1,3,5,\ldots}^{\infty} \frac{1}{n^3} (-1)^{\frac{n-1}{2}} \left(1 - \frac{\cosh \frac{n\pi y}{W}}{\cosh \frac{n\pi}{2}} \right) \cos \frac{n\pi x}{W} \tag{18}$$

where W is the length of one side of the square. Similarly

$$z_o \simeq -(0.037)\frac{\epsilon V^2 W^2}{T_o d^2} \tag{19}$$

The central deflection is not very different from that of the circular element with a diameter of W and is therefore also about one-half that of a line element of width W.

The resonant frequency equation for a square element is

$$f = \frac{1}{2W}\sqrt{\frac{T_o}{\delta t}}\sqrt{m^2 + n^2} \qquad \begin{matrix} m = 1,2,3, \ldots \\ n = 1,2,3, \ldots \end{matrix} \tag{20}$$

and

$$f_{11} = \frac{0.707}{W}\sqrt{\frac{T_o}{\delta t}} \tag{21}$$

IV. OPTICAL CONSIDERATIONS

In high-density read-write holographic memory systems, the holograms are recorded at a location on the storage medium where the light from each undeformed page composer element has been focused to a diffraction limited spot. The size of this spot is inversely proportional to the width of the page composer element. When an element is deformed by applying voltage, the light spreads over an area much larger than the hologram, and little light is recorded. In the image reconstructed from the recorded hologram, a substantial contrast is obtained between the deformed and undeformed states of the membrane. An optical system which simulates this aspect of holographic memory operation is shown schematically in Fig. 3. This configuration is a

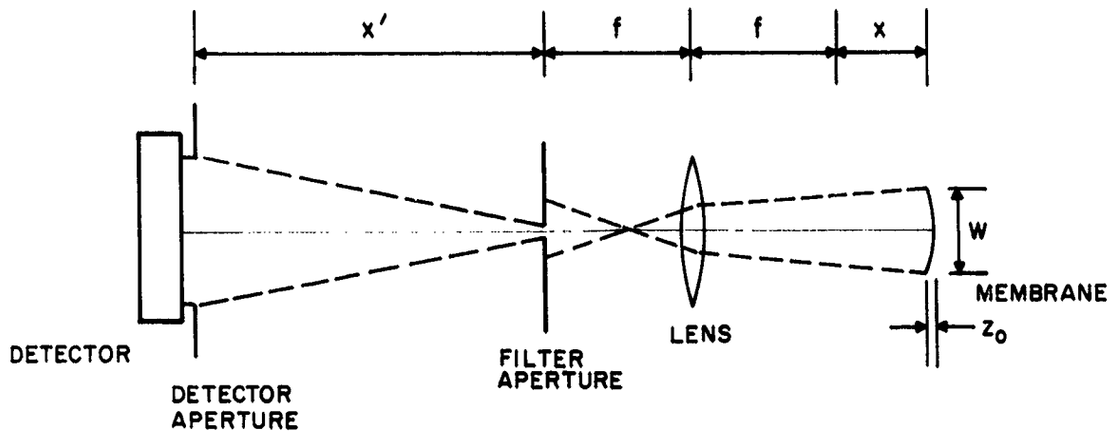

Figure 3. Simulated optical memory system.

Fourier transform filtering system having a low-pass spatial frequency response that is determined by the width of the filter aperture. With the condition $X'X = f^2$, the lens projects an image of the membrane element onto the detector aperture with a magnification $(M) = (X' + f)/(X + f)$. The detector aperture width is chosen to be MW, the size of the magnified image of the membrane element.

For this analysis of a one-dimensional line element, the light incident on the membrane is assumed to be collimated. The membrane is assumed to deform as a parabola, with a central deflection of z_o. When the membrane is undeformed, the collimated light is reflected through the lens, which focuses it to a spot small enough to pass through the small filter aperture. As the membrane deforms, the reflected light spreads over a larger area in the plane of the filter aperture, and less light is transmitted through the aperture.

First consider the geometric-optics approximation which ignores diffraction effects. The parabolic mirror formed by the membrane has a focal length (f_m) of

$$f_m \sim W^2/16\, z_o \tag{22}$$

for small deformations. The deviation of the originally collimated rays by the membrane produces a region of uniform illumination of width d in the plane of the filter aperture, where

$$d = fW/f_m \tag{23}$$

For a filter aperture of width

$$d_a = 2a\, \lambda f/W, \tag{24}$$

where a is a constant to be chosen, and λ is the wavelength of the light; the light flux I transmitted by the aperture is

$$\begin{aligned} I &= I_o\, d_a/d \qquad && d > d_a \\ I &= I_o && d \leq d_a \end{aligned} \tag{25}$$

This light forms the geometric image of the membrane element. I_o is the transmitted light flux for no membrane deflection. Combining the equations gives

$$\begin{aligned} I/I_o &= a\lambda/8z_o \qquad && z_o > a\lambda/8 \\ I/I_o &= 1 && z_o \leq a\lambda/8 \end{aligned} \tag{26}$$

With a = 1, a contrast of 8:1 is predicted for a central deflection of one wavelength by this simple analysis.

A more rigorous analysis includes the effects of diffraction caused by the finite filter aperture. The constant, a, is recognized as the ratio of the filter aperture width, to the width of the main lobe of the diffraction pattern caused by an isolated, undeformed membrane element. Over 90% of the light from an isolated, undeformed membrane would be transmitted by the aperture in this case. The image intensity distribution is given exactly by the squared modulus of the convolution of the complex amplitude of the light reflected from the membrane element, with the

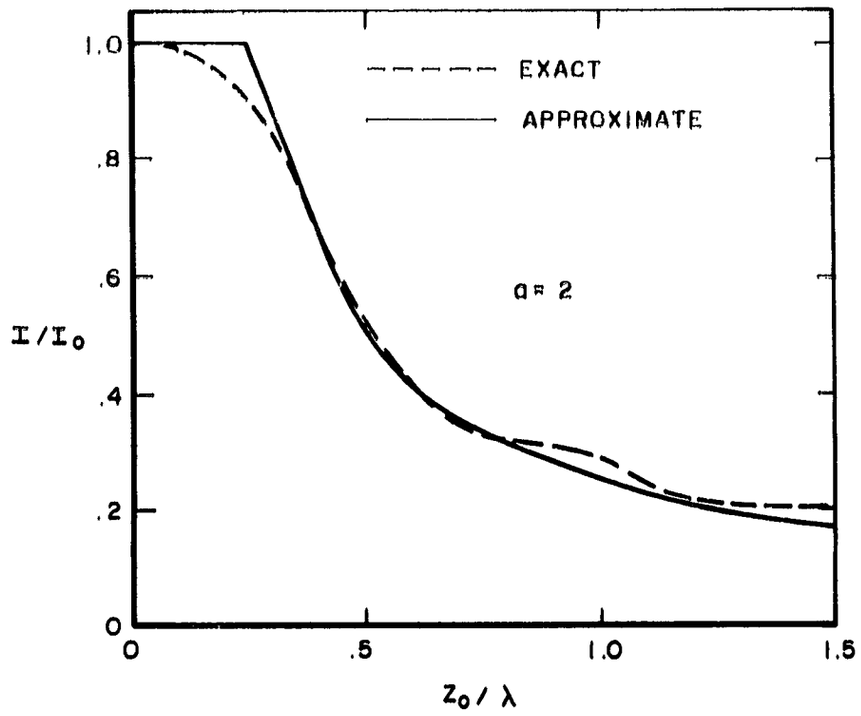

Figure 4. Detector output vs. central deflection with large filter aperture, a = 2.

point-spread function of the imaging system as set by the filter plane aperture size. This distribution is integrated over the detector aperture to give the detector output I. Figures 4, 5, and 6 show representative results of the exact analysis for a = 2.0, 1.0, and 0.5, respectively. Also shown for comparison is the geometric-optics approximation represented by Eq. (26). The approximation obviously becomes more accurate as the size of the filter aperture increases and the effects of diffraction are relatively decreased. For a given membrane displacement (z_o), the trend is generally toward better contrast for smaller filter aperture width.

The exact curves shown in the figures are for the case in which there are wide, rigid supports on either side of the deformable membrane, which are also illuminated and reflect the incident collimated light. Since diffraction by the filter aperture tends to blur the image of the sharp boundaries between deformed and undeformed regions of the reflecting surface, some of the illumination from the supports spills over into the detector aperture. This effect limits the asymptotic values of I/I_o for large deformations to 0.03, 0.06, and 0.06 for a = 2.0, 1.0, and 0.5, respectively.

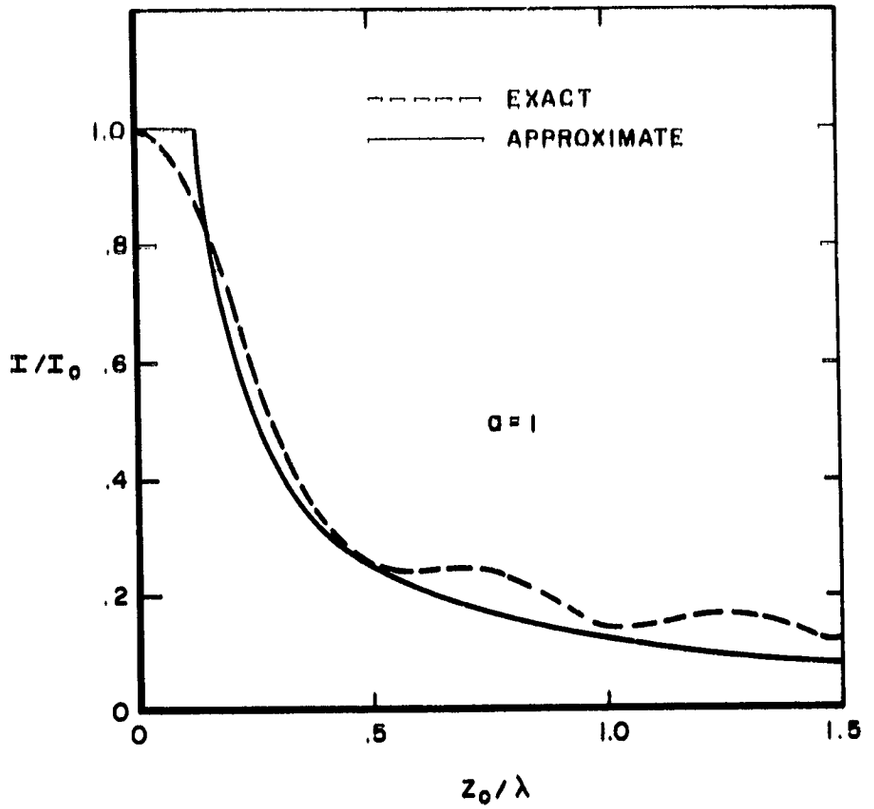

Figure 5. Detector output vs. central deflection with medium filter aperture, a = 1.

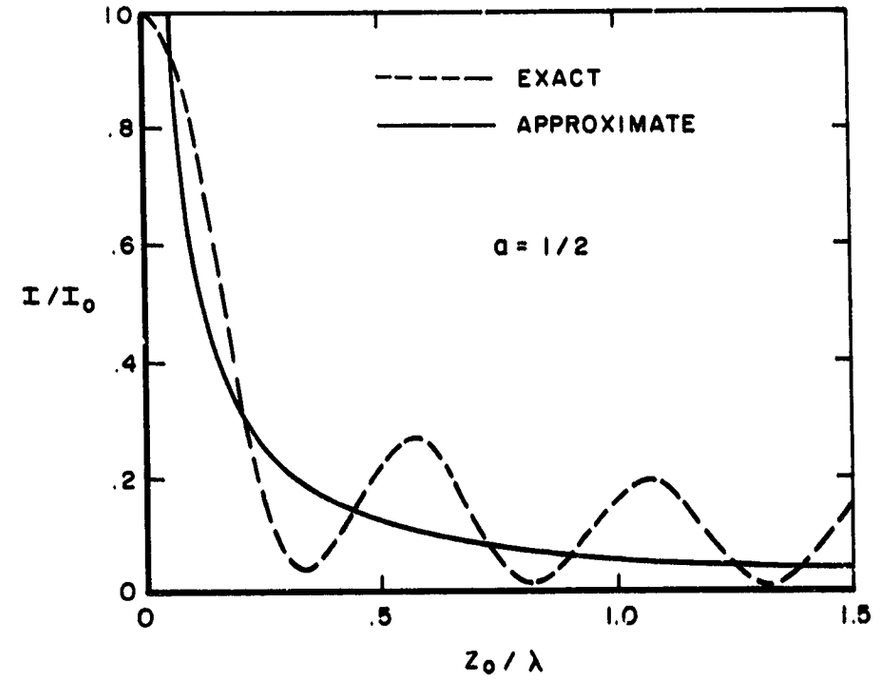

Figure 6. Detector output vs. central deflection with small filter aperture, a = 1/2.

The oscillations in the detector output as z_0 varies are caused by interference in the image between the spillover light from the supports and the phase-shifted light reflected by the deformed membrane. For the case where only the deformed region is illuminated, and no light is incident on the supports, the exact calculations show that the oscillations diminish in magnitude, contrast increases, and the curves more closely resemble the geometric-optics result. Also, as in the approximate analysis, localized illumination gives an asymptotic value of zero for I/I_0 as z_0 becomes very large.

The exact calculations have, in addition, been made to include the cases of: (a) initial flat displacement of the membrane from the level of the supports, (b) different reflectivities of the deformable membrane and the support regions, (c) lateral displacement of the filter aperture, (d) a triangular-membrane deformation profile, and (e) detector apertures different from the size of the geometric image of the membrane element. Although the detailed variation of I/I_0 with z_0 is somewhat sensitive to these additional factors, the qualitative behavior is quite similar. Of particular interest is the case of a smaller detector aperture, for which the magnitude of the oscillations increases somewhat, but the contrast for large deformations is improved by the exclusion of spillover light when the supports are illuminated.

In summary, the geometric-optics analysis provides a reasonably close first approximation to the calculated diffraction-limited performance of an idealized membrane page composer line element in the intended optical system. For small deformations, the contrast improves as the filter aperture width is reduced. However, diffraction blurring reduces the maximum available contrast as the filter aperture is narrowed when the membrane and its supports are uniformly illuminated. This degradation is reduced by narrowing the detector aperture, and is eliminated by restricting the incident illumination to the deformable region of the element only.

V. MEMBRANE LIGHT VALVE FABRICATION

The membrane light valves of various geometries previously described have many features in common such as a substrate, an electrode pattern, a support-structure pattern, and a thin metal film over the support structure. In this section, a description of typical processing used in fabricating an MLV is given.

First, the substrate is thoroughly cleaned by finger-rubbing with deionized water and isopropyl alcohol in various sequences and then blown dry. In a dust-free hood, Shipley AZ1350 photoresist is then applied in drops and is distributed evenly over the surface with the dropper. After allowing the resist to dry for 1 hour, the substrate is placed on a hot plate at 55°C for 3-4 hours. Then the substrate is aligned and registered with a photomask. The photoresist is exposed with ultraviolet light through the mask, after which the pattern is developed with Shipley AZ1350 developer. Then the substrate is rinsed well and checked for complete removal of the exposed resist.

The electrode material (usually a chrome flash followed by about 0.7 μm of aluminum) is then deposited over the whole area of the substrate, landing on the substrate surface in the exposed regions and on the photoresist elsewhere. If insulated electrodes are desired, silicon monoxide can be put down over the aluminum. In the next step the desired pattern is formed by placing the substrate in a bath of solvent which strips away the photoresist. If the height of the resist is chosen to be about 3-5 times greater than the desired thickness of electrodes, and sharp walls of the pattern lines are exposed and developed properly, then the resist will wash away taking with it the material deposited on it, and the thin webbing on the walls of the resist connecting the top of the resist with the material deposited on the substrate. Acetone is the usual stripper for Shipley resist and works rapidly. A mix of alcohols is also effective and although slower acting, is more compatible with some materials. After the resist is washed away, what remains is the pattern of electrodes which was formed by the material landing on the substrate rather than on the photoresist. With this technique, the fact that a pattern can be created without the need to etch away unwanted material is a distinct advantage for certain kinds of processing.

The support structure must be made next. This may be either SiO or metal (aluminum) and is formed by the use of the same photolithographic techniques employed to make the electrodes — namely exposing and developing a pattern in photoresist, depositing the appropriate material over it, and then stripping the photoresist, leaving the desired support structure geometry.

Now the substrate is ready for the membrane, but some intermediate steps are necessary. Shipley AZ119, a thick resist, is used as a temporary substrate on which to deposit the membrane

after which the resist can be removed leaving the thin film suspended on the supports. To accomplish this, the resist is applied in drops distributed uniformly over the substrate by spinning slowly, and made thick enough to be higher than the support structure. Next, the resist is dryed overnight on a hot plate at 55°C, after which it is ready to be polished. The thick layer of resist is polished until just enough resist has been removed so that all of the support structure surfaces are visible and level with the resist elsewhere. The remaining processing should be done as quickly as possible to avoid sagging or distortion of the resist on which the membrane will be deposited.

The next step is necessary in order to be able to remove the photoresist layer after the membrane is completed. Basically the technique is to incorporate tiny micrometer-sized holes into the membrane so that the resist solvent can go through the membrane and carry out the resist with it. To form the holes a gelatinous solution is first poured over the substrate, and then rinsed off with deionized water leaving a thin film of gel. Then, with the substrate still wet, a dispersion of micrometer-sized ZnS in water with sodium pyrophosphate added is poured over the substrate and allowed to settle. Then the substrate is gently rinsed with deionized water and blown dry, leaving a uniform distribution of particles over the resist and support structure anchored in gelatin. The substrate is placed in a vacuum system where a flash of aluminum (0.06 μm) and nickel (0.08 μm) is sequentially evaporated. The combined thickness of metal is not sufficient to cover the particles on the substrate surface. Therefore, when the sample is removed from the vacuum system and gently wiped with wet tissue, the tiny particles are dislodged and are then removed by a rinse with deionized water leaving holes in the metal where the particles had been.

The evaporated metal film with holes is used as the seeding layer on which to plate the full thickness desired of the nickel membrane. The sample is placed in a holder which serves as the cathode in a nickel-plating bath. Good electrical contact between the holder and the flashed film on the sample surface is essential. With the bath temperature at 110°F, currents of 0.75 to 2.0 A and times of about 1 — 2 1/2 minutes, good films in the thickness range of 0.4 to 0.8 μm have been made. Various current-time combinations are possible to control both thickness and tension in the plated-nickel films.

The final step involves removal of the photoresist beneath the membrane surface which has served as a temporary substrate. The sample is taken from the plating bath, rinsed with deionized water, and blown dry. Two dishes of solvent bath are used in sequence. The sample is immersed in the first dish of solvent which gets to the resist through the tiny holes in the nickel film and diffuses out of the region. This procedure is repeated in the second dish. A critical concern is that the liquid beneath the membrane after the resist is dissolved does not tear the membrane or distort it as it dries. For this reason, a final bath of hot ether is employed prior to the drying of the sample. This technique has been successful in producing flat films for the membrane light valve elements.

VI. THE NASA 8 × 8 PAGE COMPOSER ARRAY

All of the foregoing involved membrane light valves without concern for how array operation can be attained. Since a light valve element does not have true threshold or memory properties, these must be provided at each bit location by other means. We have chosen semiconductors for this purpose. Static storage is obtained with flip-flops at each bit, while dynamic storage is possible if MOS transistors are used as gates at each bit to control the charge and discharge of the membrane-electrode capacitance. Still remaining, is the problem of connecting each element electrode to the semiconductor circuitry. Since, in a large array, it is impossible to bring out leads from each element, we make use of feedthrough connections in the substrate itself leading from electrodes on one side to the semiconductor drivers on the opposite side of the substrate. Interconnections and pads for external wires to the control and selection electronics can also be included on the backside of the substrate, and semiconductor chips can be beam-lead bonded at the appropriate locations

The three major parts of the NASA device will now be described. First is the membrane light valve array. This consists of circular elements, 0.75 mm in diameter, spaced on 1.5-mm centers. One variation involves making 0.75-mm-square elements, each of which is subdivided into a 3 × 3 subarray of 0.25-mm-square elements. This multiple-element light valve has the attractive features of redundancy and ease of fabrication. The method of fabricating the light valves on a substrate that has already been described is also applicable to the 8 × 8 array.

The substrate with feedthroughs is the second major part of the device. After studying several alternatives, we chose Fotoform or Fotoceram materials which are manufactured by Corning Glass Works. This glassy material can be exposed with ultraviolet light passing through a mask, and can be subsequently developed and preferentially etched to close tolerances. Holes etched through the thickness of the substrate can then be filled in with conductive material by various techniques. We have successfully used several kinds of silver epoxy for this purpose. The advantage of the Corning material is that regular patterns can be etched which register precisely with other patterns needed for fabrication of the device. The glassy substrate can also be converted into a tough ceramic-like form by a final heat-treatment step. The substrate thickness is about 1.25 mm.

The third major part of the NASA device includes the semiconductor chips, the metallization patterns and their interconnections on the backside of the substrate. A novel method of obtaining dynamic storage was devised utilizing a single MOSFET gate at each element. This simplifies the circuitry on the semiconductor chip and the back-plane wiring considerably over what would be needed if flip-flops were used. In addition, by designing the chip to include "carry-overs" which bridge interconnection lines on the substrate on either side of the chip, only a single layer of metallization is needed on the backside of the substrate. Each chip includes four transistors, each of which controls one light valve so that only 16 chips are needed for the 8 × 8 array.

As an intermediate step, devices were made with light valves and substrates as described, but with a metallization pattern on the backside which brought out each feedthrough to a connection pad, to which an external wire could be connected. This device allowed testing and evaluation of the light valve – substrate combination to proceed without the semiconductor circuitry which was to be added later. In the meantime, the Solid State Technology Center at RCA Somerville was designing the semiconductor chips to our specifications which included a 50 V minimum breakdown voltage between any two transistor terminals, 1 μsec switching speed, and the appropriate beam leads for each chip to be bonded to the substrate in registry with our interconnection patterns.

A clearer picture of the NASA device can be obtained by considering the details of a 4 × 4 array for illustrative purposes. Figure 7 shows the development of such an array. In the final fabrication sequence, step (e) precedes step (d) because the membrane is the most delicate component of the device and is therefore put on last. Figure 8(a) shows a pictorial representation of Section AA of Fig. 7. The backside of the substrate is shown in Fig. 8(b) with the chips in place. Figure 8(c) shows a schematic layout of the transistors and the wiring on a single chip. Two other views of the chip on the substrate can be seen in Fig. 9. Note that the chip is suspended above the surface of the substrate by the beam lead connections. Also note that the X and GND leads run beneath the chip to continue across the substrate, while the Y leads are continued across the substrate by means of a bridge or tunnel on the chip itself. The actual chip size is 1-mm square, while the conducting lines are 0.125-mm wide. A 4 × 4 array of square elements is shown in Fig. 10(a) while Fig. 10(b) shows a square multiple-element light valve. Note that one electrode controls four subelements. The insulation layer over the electrode assures that a torn piece of membrane in a subelement does not short out other subelements by touching the common electrode.

As can be seen in Fig. 8(c), an X line is connected to one row of MOS gates while a Y line is connected to one column of drains. The source of each MOS is connected to a respective feedthrough. In operation, an X or word line is activated causing the MOS channel to be conductive. The desired voltage pulse (1 or 0) on each Y line then appears at the corresponding feedthrough electrode, and acts on the grounded membrane of that element accordingly. With the gate disabled before the data pulse ends, the charge on the capacitance element formed by the electrode-membrane combination will leak off slowly in a time determined by the leakage current of the transistor. This current can easily be made small enough for storage times of many milliseconds. As long as the cycle time of the page composer is short compared to the leakage time, or if refreshing of the array is allowed, then effective memory is obtained with this technique.

The actual 8 × 8 array layout can be seen in Fig. 11: The array of light valves on the front side of the substrate is seen in the sample at the top of the photograph. The bottom left sample shows the wiring and the chips on the backside while the bottom right sample shows the backside wiring for a device with individual access wires. The layout on each chip is seen in the photograph of Fig. 12(a), while the chip in place on the substrate with its connections is seen in Fig. 12(b).

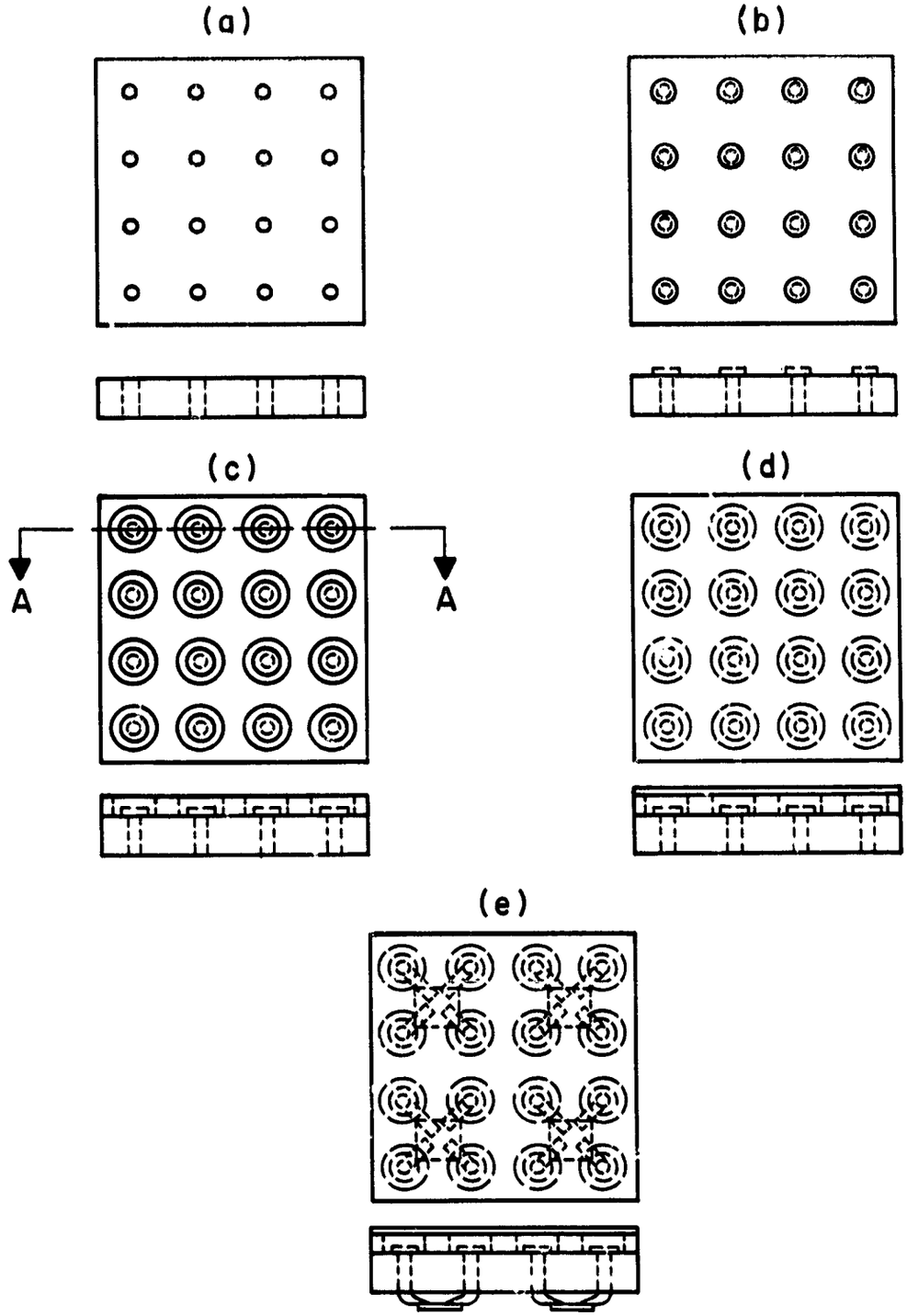

Figure 7. Sequential steps in the development of a 4 × 4 array of membrane light valves.
(a) Fotoceram substrate with holes.
(b) After filling holes with conductive material and forming electrode caps.
(c) After forming a support structure.
(d) After adding membrane.
(e) After bonding semiconductor chips to backside of substrate.

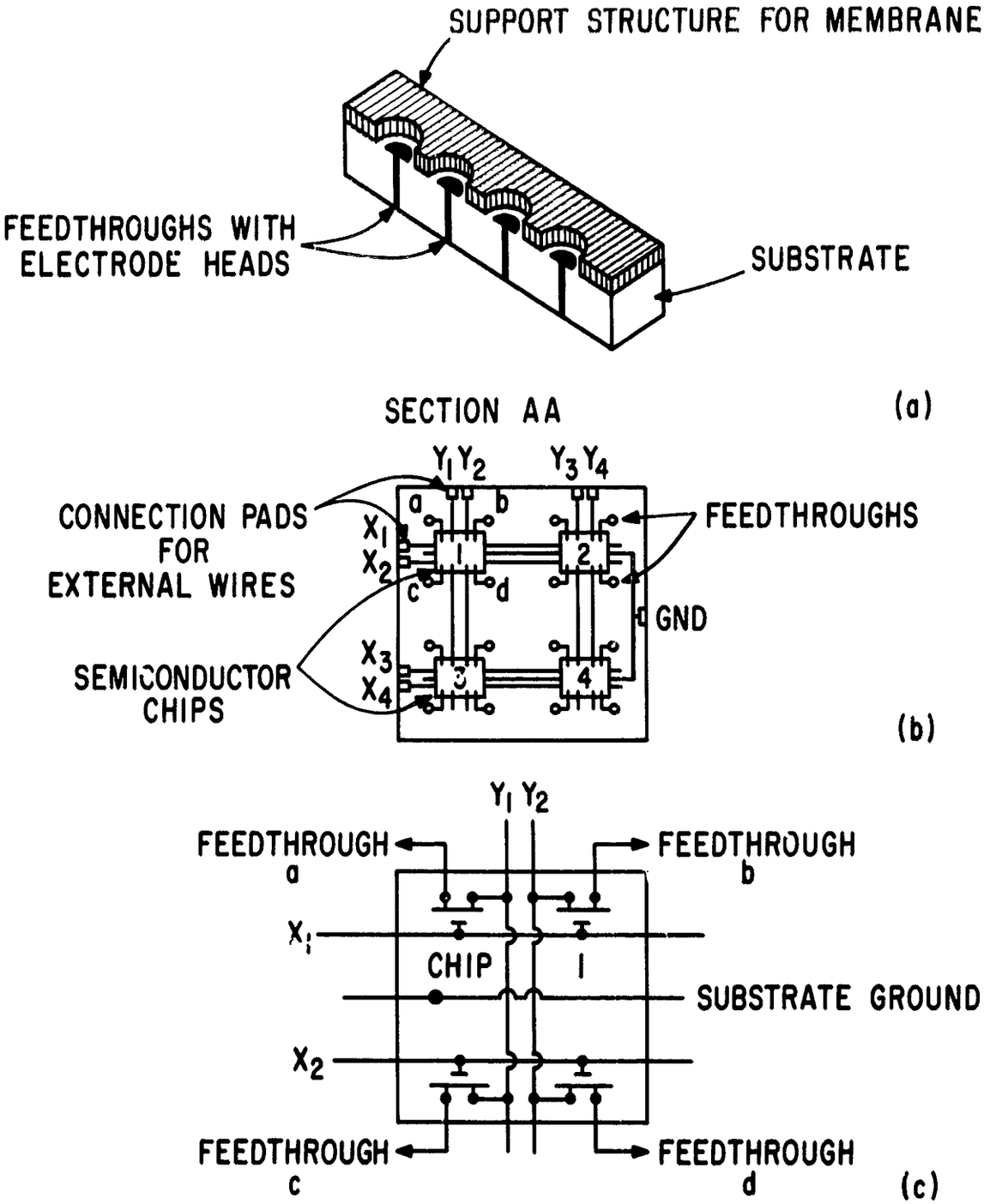

Figure 8. (a) A pictorial representation of Section AA of Fig. 7(c).
(b) A schematic representation of the backside of the substrate showing the semiconductor chip in place and its associated wiring.
(c) A schematic representation of a semiconductor chip showing 4 MOS transistors and their associated wiring.

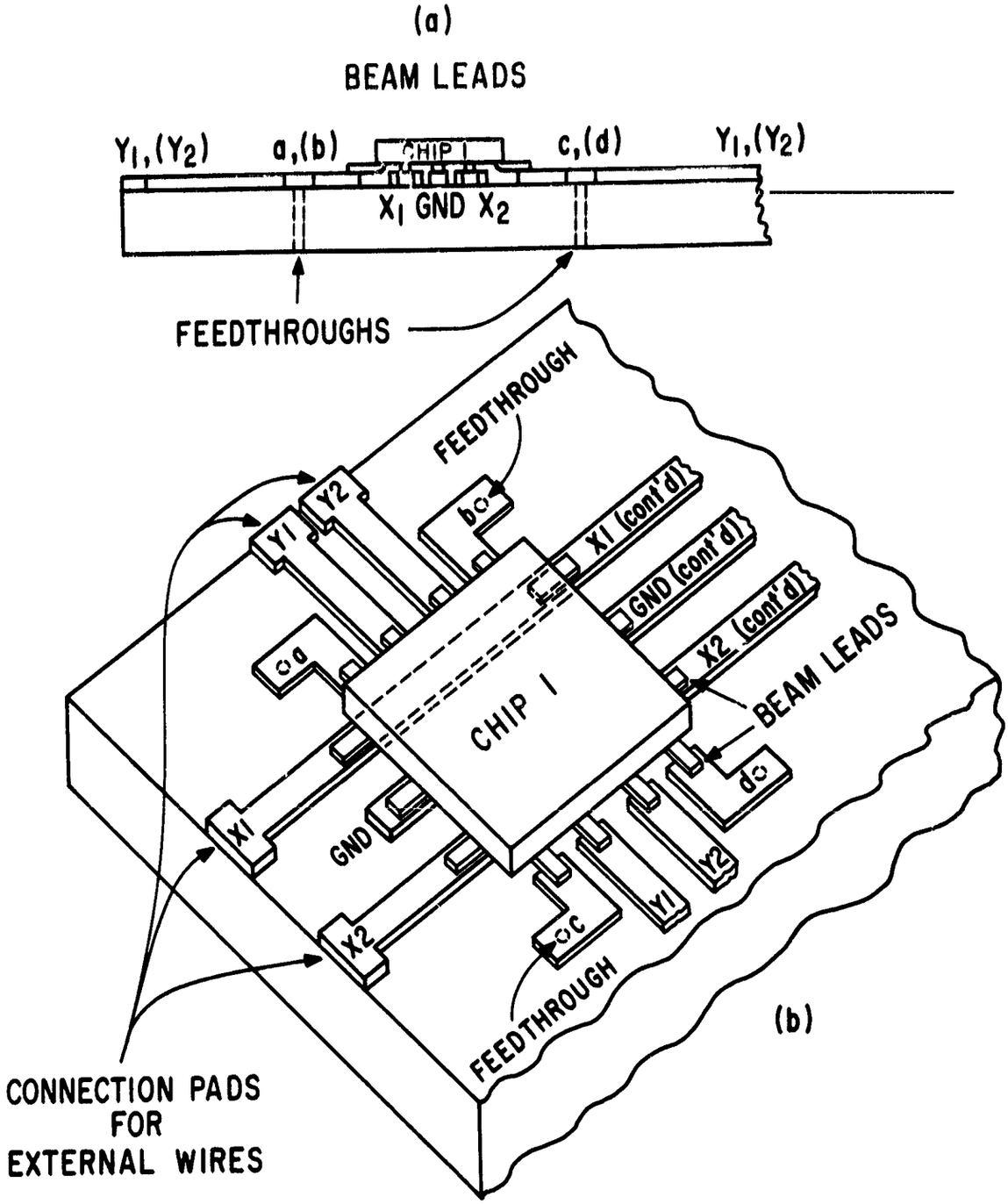

Figure 9. (a) A detailed view of a semiconductor chip and its associated leads on the backside of the substrate.
(b) A pictorial view of the chip on the substrate.

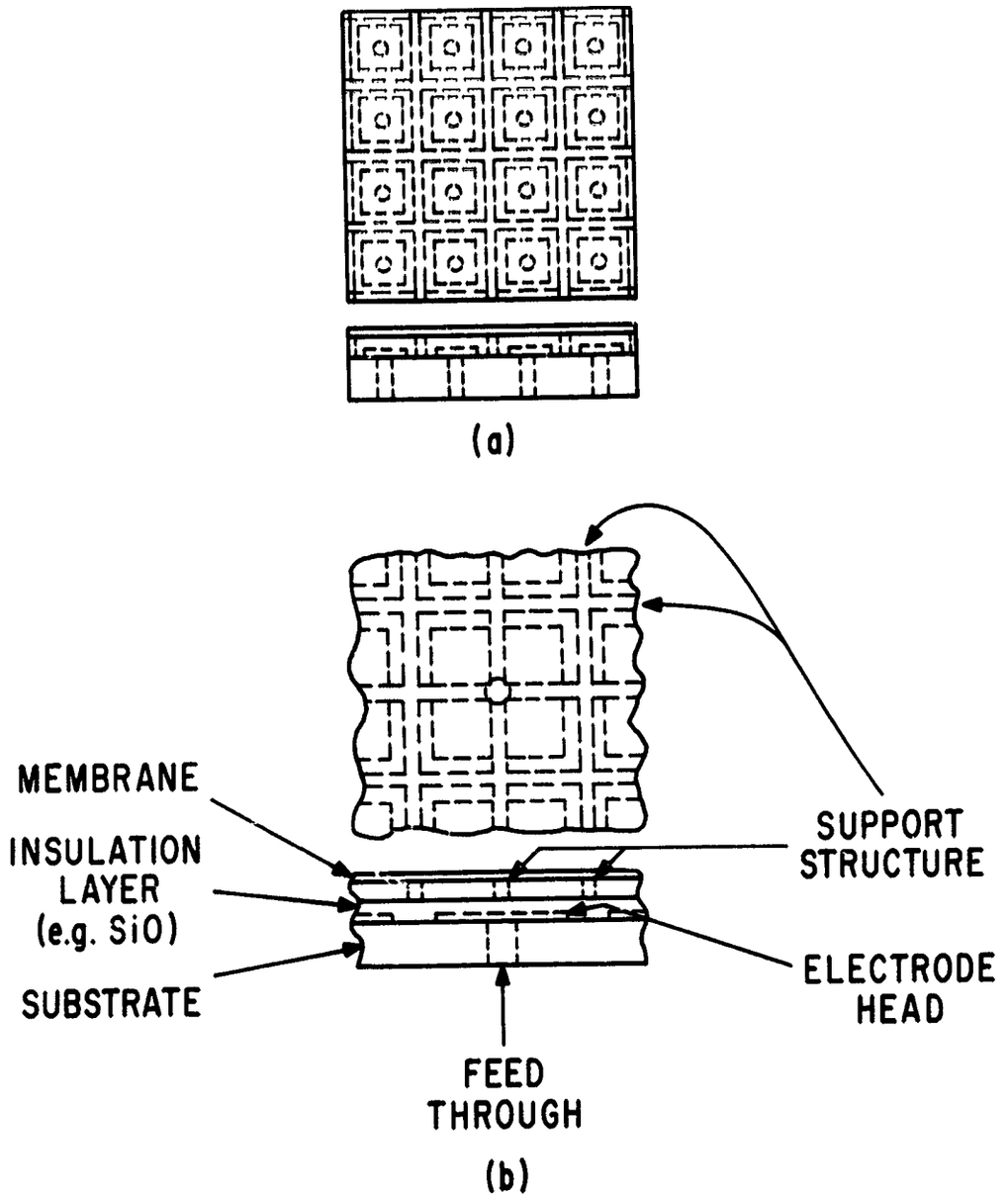

Figure 10. (a) A 4 × 4 array of square-element membrane light valves.
(b) A square multiple-element membrane light valve made up of a 2 × 2 array of individual elements.

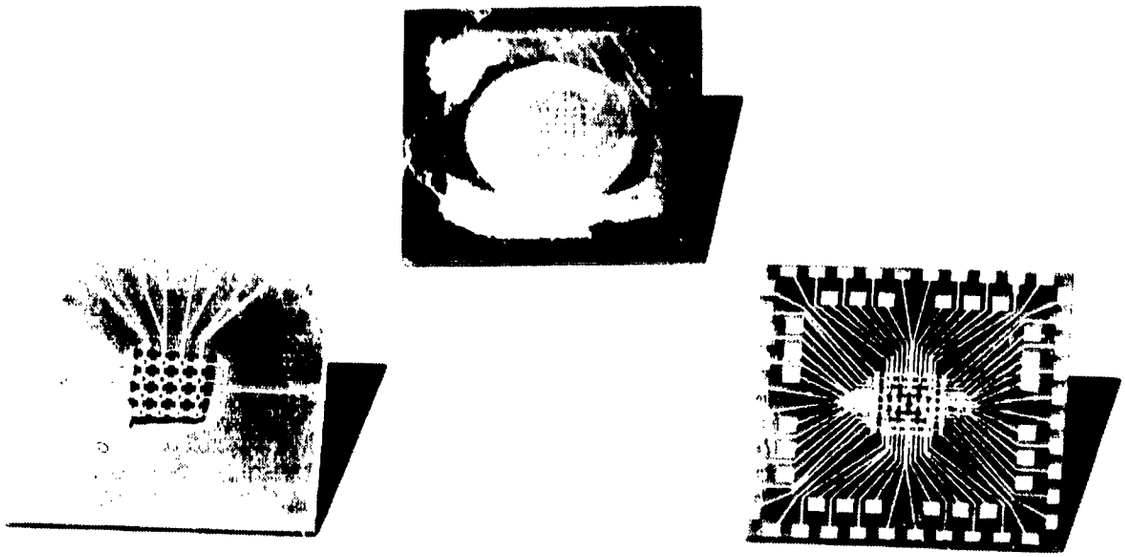

Figure 11. NASA 8 × 8 arrays.

Three practice fabrication runs were made using Fotoceram substrates. First, feedthroughs and support structure were added to the substrates. RCA Somerville then formed the backside metallization pattern and beam-lead bonded "dummy" semiconductor chips at the appropriate locations, and encapsulated the chips on two of the samples. (The chips were mechanically the same as the actual chips but did not have transistors on them.) Finally, we added the membranes to complete the devices. These dry runs served to identify potential areas of incompatibility in the overall fabrication process. After all such difficulties were resolved, a fabrication sequence for the final device was established.

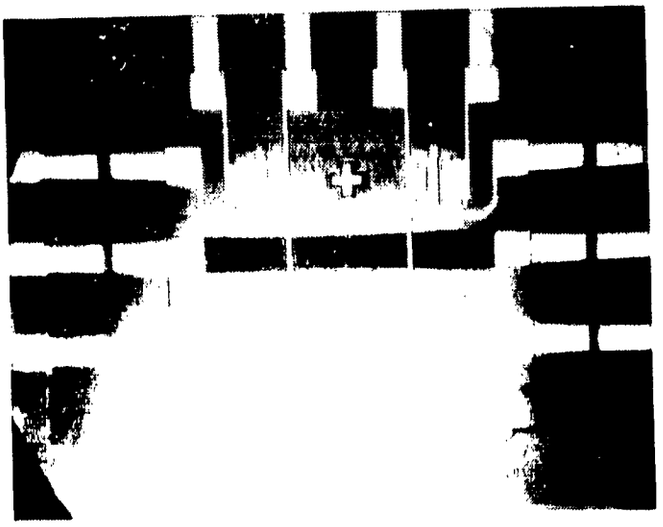

(a)

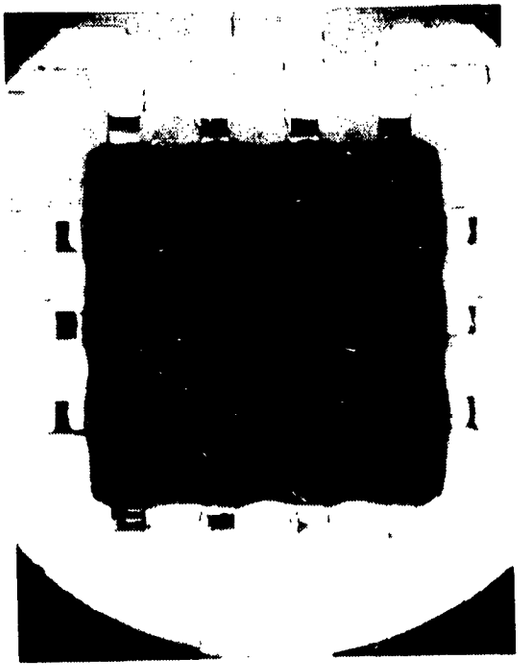

(b)

Figure 12. (a) Layout of MOS transistors and beam leads on a chip.
(b) Chip with beam lead connections in place on a substrate.

VII. EXPERIMENTAL RESULTS

A. Line Elements

Early experiments with membrane line elements were made to determine the separation between membrane and electrode, and the metal membrane thickness needed to obtain deflections sufficient to produce a contrast ratio of about 10 at the detector with an applied voltage of 50 V or less. The test vehicle used for this purpose was a sample on a 5-cm by 5 cm glass substrate with nine line elements of the type shown in Fig. 1(a), except that wide supports (~ 3 mm) were used between elements. Each cell was about 0.25 mm wide with electrodes half as wide. It was found to be advantageous to deposit silicon monoxide over the line electrodes to prevent a local defect from shorting out the entire line element. Dozens of such samples with numerous variations were made. Electrical and optical properties of the line elements were determined and recorded. Different materials, either evaporated or plated, were tried for the membrane, but because of early success with plated nickel films most of the samples were made with this type of membrane.

After a visual inspection of the sample, checks were made of electrode continuity and for shorts between membrane and electrodes. Next, data were taken in the simulated optical memory system of Fig. 3, with a helium-neon laser light source and a photomultiplier tube detector. Usually, the detector aperture was about the size of the geometric image and the filter aperture was about equal to $2\lambda f/W$. The light intensity at the detector (I) was measured as a function of the applied voltage, and photos such as that of Fig. 13 were taken, from which contrast could be determined.

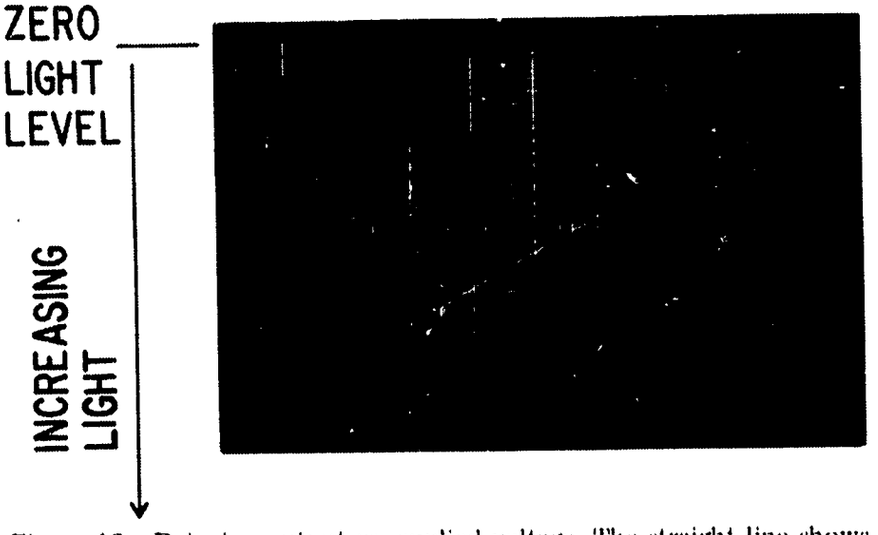

Figure 13. Detector output vs. applied voltage. The straight line shows the sawtooth voltage, while the curved waveform shows the light variations. The voltage scale is 20 V/div. The data are for line 3 of sample R-161 which had a membrane 0.36 μm thick and a support structure 1.2 μm high.

For all such photos, the zero light level is at the top line of the graticule and light intensity increases in the direction shown. Also, the scope sweep speed is always 5 msec/div., unless otherwise noted. Data from interferometer measurements were used to plot the central deflection (z_o) as a function

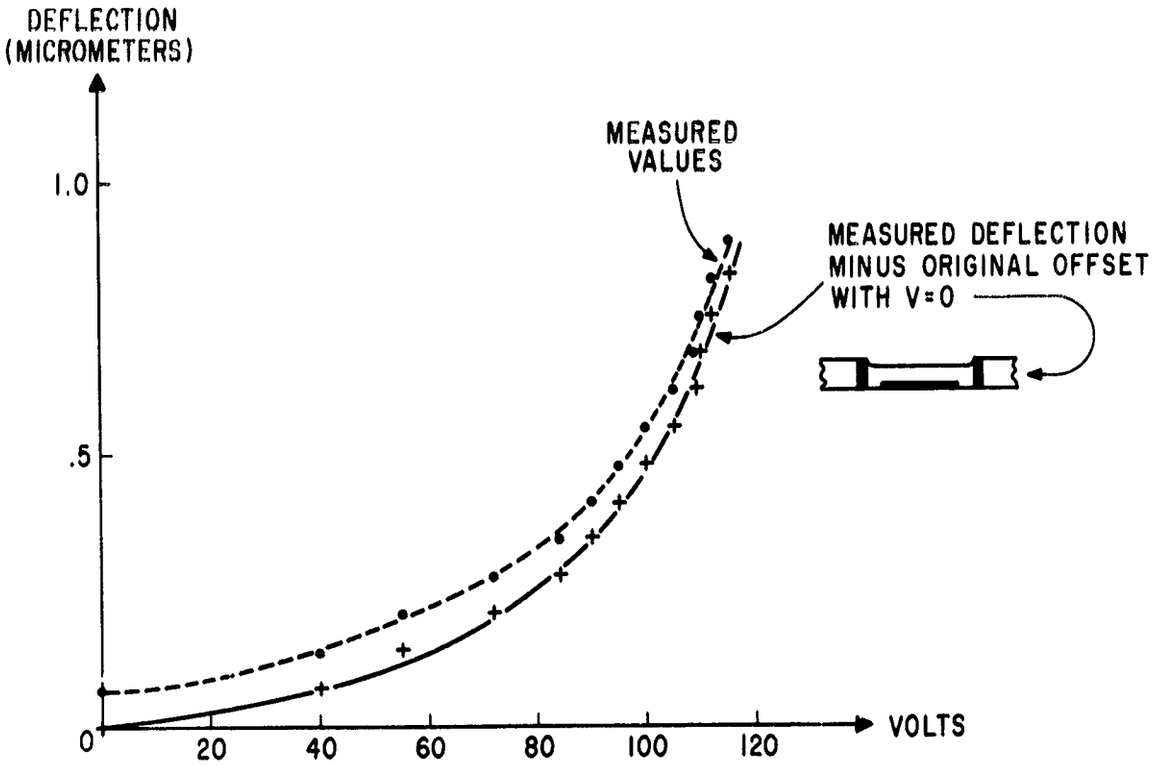

Figure 14. Deflection vs. voltage for line 3 of R-161.

of applied voltage as seen in Fig. 14. The same data have been replotted on log-log scales in Fig. 15. The plated-nickel membrane was typically quite flat, but was located below the support structure surface by about 0.1 μm or less, as indicated on Fig. 14. This probably occurred when the photoresist was polished before the membrane was put on. Since the resist is softer than the support structure it would polish faster, resulting in an undercut of the type seen. Another contributing factor might be a slight sagging or shrinkage of the resist after polishing and before the membrane is deposited. Because the membrane surface is quite flat, however, the small offset from the surface of the support structure does not introduce significant problems. By combining the two previous sets of data, I versus z_o could then be determined as shown in Fig. 16.

Test samples were fabricated with support heights ranging from less than 2 to more than 6 μm. Membrane thickness ranged from 0.18 to over 0.5 μm. The best results obtained from these elements were well within our requirements. For example, one sample produced a 15:1

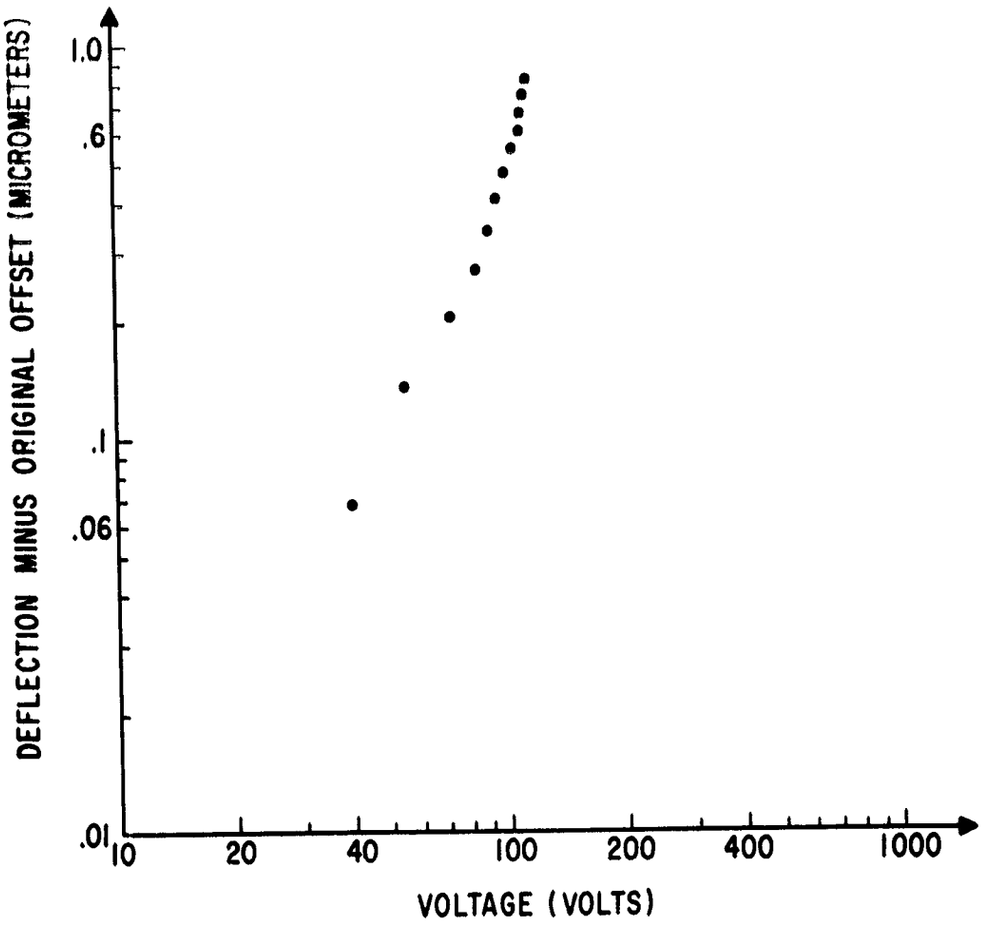

Figure 15. Deflection vs. voltage for line 3 of R-161 replotted on log-log scales.

contrast with 40 V applied. Several others showed a contrast of about 10:1 with applied voltages ranging from 25 to 50 V. The favorable performances indicated that a line element with a plated-nickel membrane about 0.4-μm thick, and a membrane-to-electrode spacing of about 2 μm would meet our goals, while maintaining a reasonable yield from the fabrication cycle.

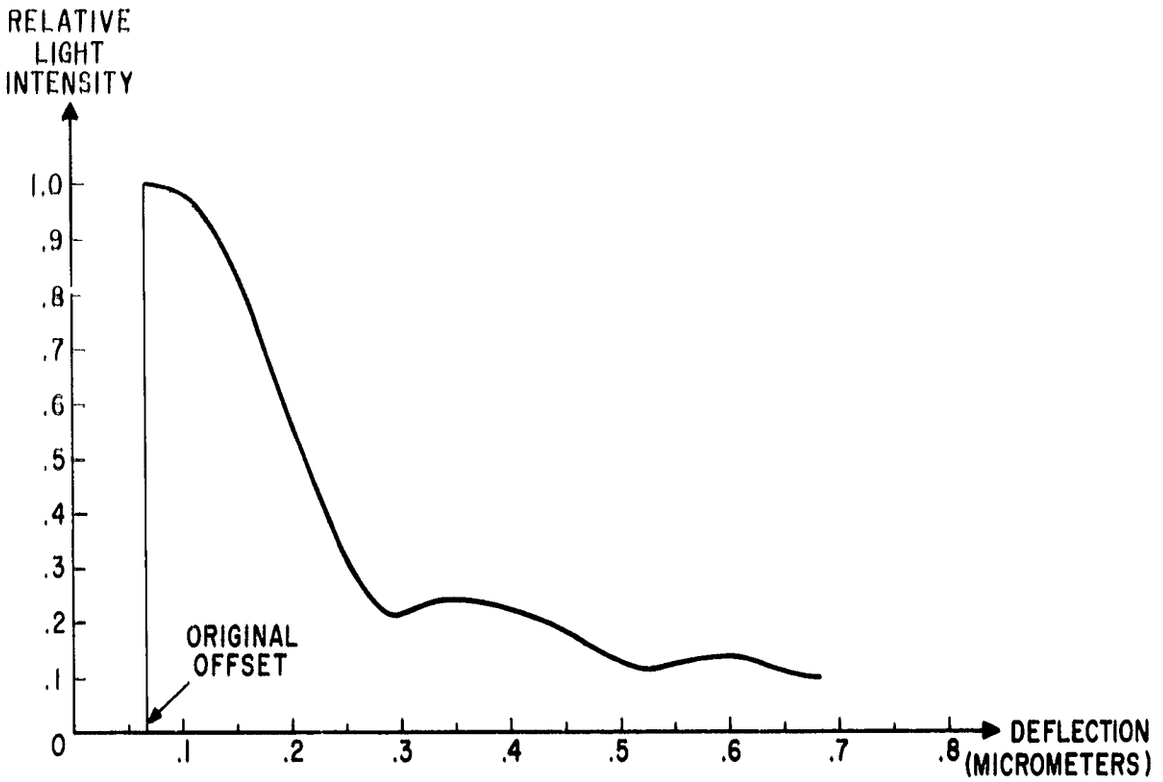

Figure 16. Detector output vs. deflection for line 3 of R-161. This plot was made by combining the data of Fig. 13 with the curve of Fig. 14 drawn through the deflection values as measured from the support structure height.

Some other data obtained from line elements are shown in Fig. 17. Light intensity versus voltage is seen for three samples in (a), (b), and (c) of that figure. Pulse experiments were also run to determine switching speed and fatigue behavior of the elements. The pulse response in air of one element is shown in Fig. 17(d). Another element of this sample was cycled 189×10^6 times (5 hours and 15 minutes of pulse excitation at 10 kHz). No change was discernible either in the light reflected from the element, or in the appearance of the element itself after excitation, indicating that fatigue effects, if any, are small.

Switching of a line element was done both in air and in a pumped-out enclosure. Operation is slower in air because of the molecules which must be squeezed out from the space beneath the membrane as it deforms. An early sample (MC7) with an evaporated aluminum-zinc membrane 0.60-μm thick and 6.5-μm high support structure was pulse excited in vacuum and caused light oscillations at 330 kHz. By using a slower rise time excitation pulse (e.g. 10 μsec), the amplitude of the oscillations could be reduced to very small values. More results in vacuum were obtained

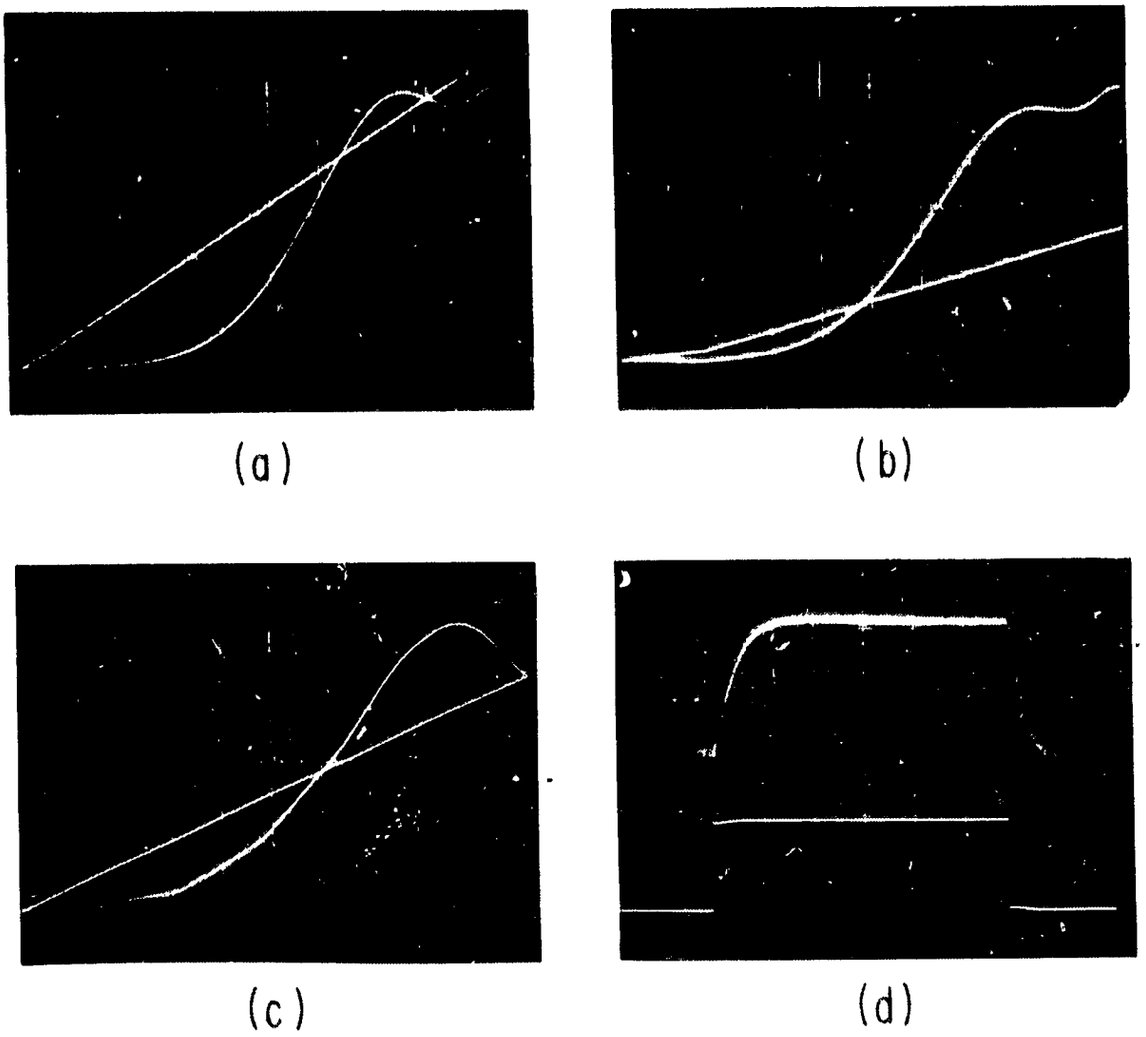

Figure 17. Detector output vs. applied voltage. The voltage scale is 20 V/div. for all photos except (c), where it is 10 V/div.
(a) Line 5 of R-172 which had a membrane thickness (t), of 0.4 μm and a support structure height (d), of 4.0 μm.
(b) Line 3 of R-178 for which t = 0.22 μm and d = 3.3 μm.
(c) Line 1 of R-239 for which t = 0.5 μm and d = 3.3 μm.
(d) Pulse response of line 4 of R-238 for which t = 0.4 μm and d = 3.15 μm. The top waveform shows the detector output with the bottom voltage pulse applied. The horizontal time scale is 20 μsec/div. for this photo.

with other types of elements which will be described later. In air, the same line element of MC7 was seen to have a fast region of response followed by a slower tail as the air was forced out of the element space.

B. Square Elements

Membrane elements 0.25-mm square were fabricated on a two-dimensional grid structure made on a 5-cm by 5-cm glass substrate. Line electrodes were formed to be 0.15-mm wide, and to run in one dimension only under one row of square elements. A silicon monoxide blanket about 1-μm thick was deposited over the substrate to insulate the electrodes from the aluminum support structure which was about 1.25-μm thick. Except for a few shorts, there were no problems with this technique and adhesion of the supports to the SiO was good. The membrane was plated nickel about 0.4-μm thick. Three samples of this type were extensively tested. Data was taken for 0.25-mm-square elements activated by a single line, and also for simulated large 0.75-mm-square elements composed of a 3×3 group of the 0.25-mm-square elements, and activated by energizing the three line electrodes beneath that group simultaneously. Several elements of each kind were tested on every sample. In the simulated optical memory system, the average contrast measured for the single elements tested was 10.4 at an average applied voltage of 33.1 V, with an aperture in the focal plane of the imaging lens of about 1 mm diameter. This aperture is large enough to let through the first order light of the support grid structure. With the aperture reduced to 0.8-mm diameter to exclude the first order light from the image, contrast increased substantially — as much as a factor of 2 in some cases. Contrast as high as 20 was obtained for a single element for this case. Simulated multiple-element light valves were also found to operate with a contrast of 10 or greater at voltages below 50 V, with various aperture sizes at the focal plane of the imaging lens, thereby meeting our performance requirements. Another test was run on a single-element valve using a fixed focal-plane aperture of 1-mm diameter and various aperture sizes at the detector. The results are shown in Fig. 18. It can be seen that in the range measured, the contrast improves as the detector aperture is decreased. The highest contrast of 30 was obtained with an aperture about 0.68 times the nominal image size. Of course, a reduced detector aperture also means reduced light at the detector but a trade-off might be desirable in some cases.

A curve of light intensity versus voltage for one square element is shown in Fig. 19(a), while the pulse response of an element is shown in Fig. 19(b). Corresponding pulse responses of elements from two other samples are shown in Figs. 19(c) and (d). Note that in air, the rise time for the three elements varies from less than 10 μsec for one element, to 200 μsec for another. The response in vacuum of three elements is seen in Fig. 20, which clearly shows the oscillations in the reflected light from the membranes as they mechanically vibrate. Note that the resonant frequencies range from 530 kHz to 610 kHz, which is a small variation compared to that of the responses in air. The reason for this appears to be that the response in air is dependent on the

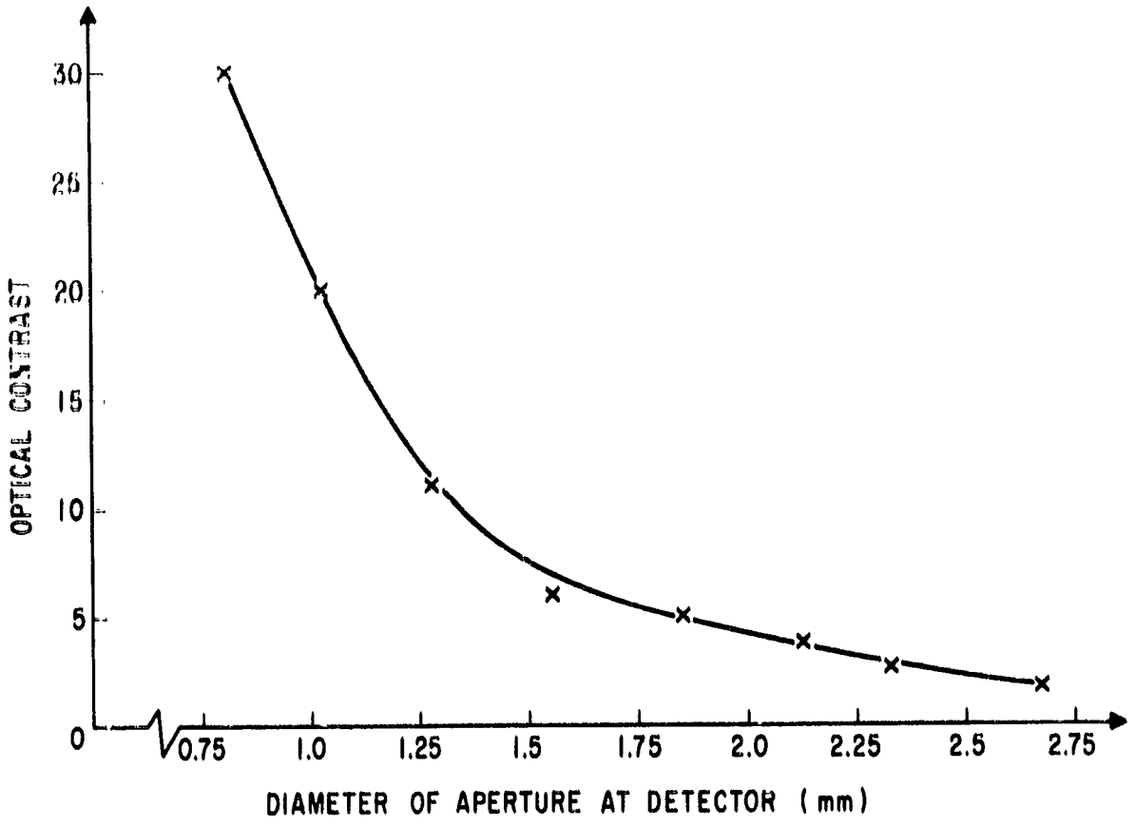

Figure 18. Contrast vs. detector aperture size for one square element on line S1 of sample 2D-5.

number of micrometer-sized holes in the membrane of an element, which are a by-product of the fabrication process. The greater the number of holes, the faster is the response — presumably because of less damping in air. A microscope inspection of the samples showed that 2D-5 had the greatest number of holes per unit area, 2D-3 had fewer holes per unit area, and 2D-4 had the fewest holes per unit area, supporting the above hypothesis. More results of excitation in vacuum are shown in Fig. 21.

C. Circular Elements

Membrane elements 0.75-mm in diameter were made only on Fotoform — Fotoceram substrates with feedthroughs. They were accessed by individual wires connected to the metallization pattern on the backside of the substrate, which brought out a conductor from each feedthrough to a pad. In this respect, the circular elements differ from th se of the line and square elements,

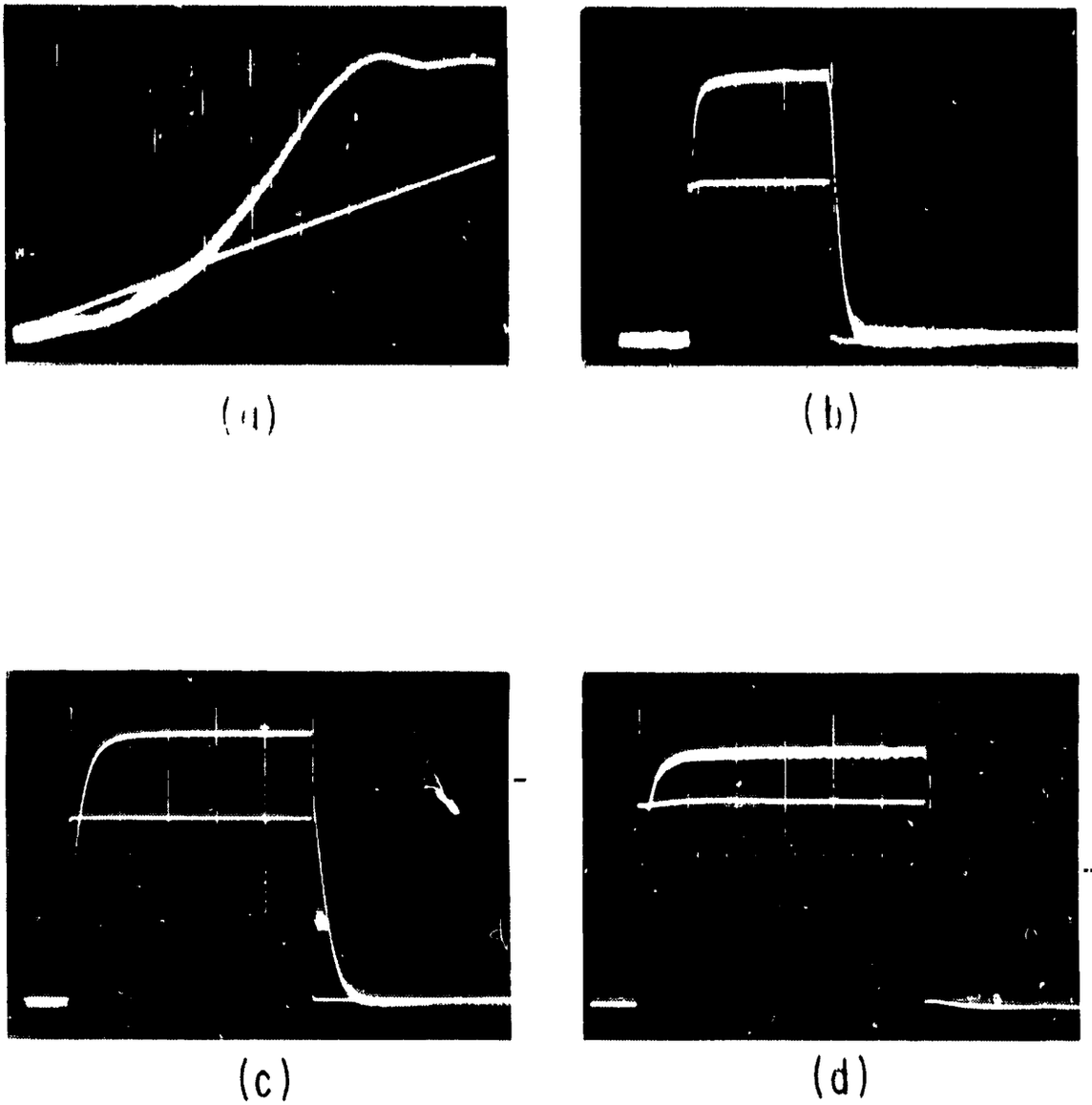

Figure 19. Detector output vs. applied voltage. The voltage scale is 10 V/div. for all photos.
(a) An element of line S1 on sample 2D-3.
(b) The pulse response of an element of line S1 on 2D-3. The time scale is 50 μsec/div. The applied voltage pulse is shown on the same base line as the light output.
(c) An element of line S1 on 2D-4. The time scale is 200 μsec/div.
(d) An element of line S1 on 2D-5. The time scale is 10 μsec/div.

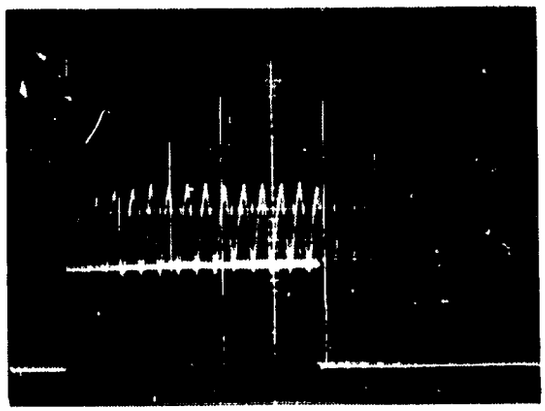

(a)

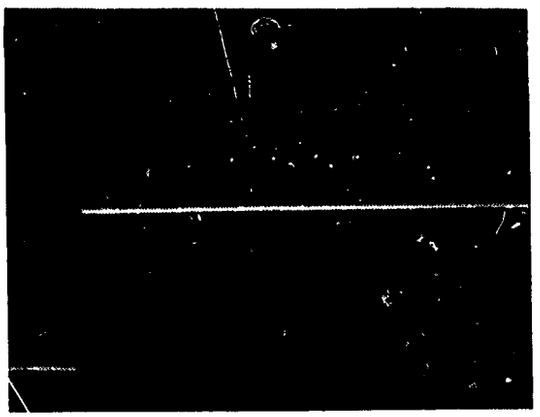

(b)

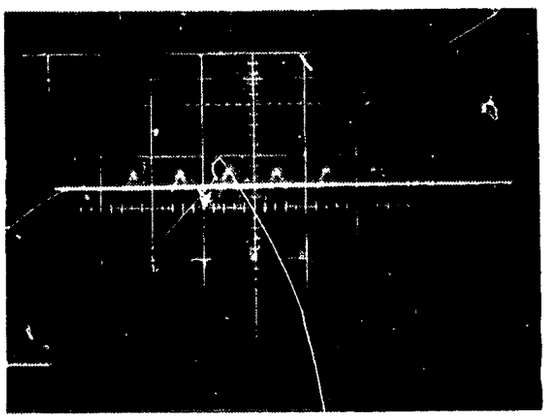

(c)

Figure 20. Pulse response in vacuum. The voltage scale is 10 V/div. for all the photos.
(a) An element of line S1 on 2D-3. The time scale is 5 μsec/div., f_{11} = 580 kHz.
(b) An element of line S1 on 2D-4. The time scale is 2 μsec/div., f_{11} = 610 kHz.
(c) An element of line S1 on 2D-5. The time scale is 2 μsec/div., f_{11} = 530 kHz.

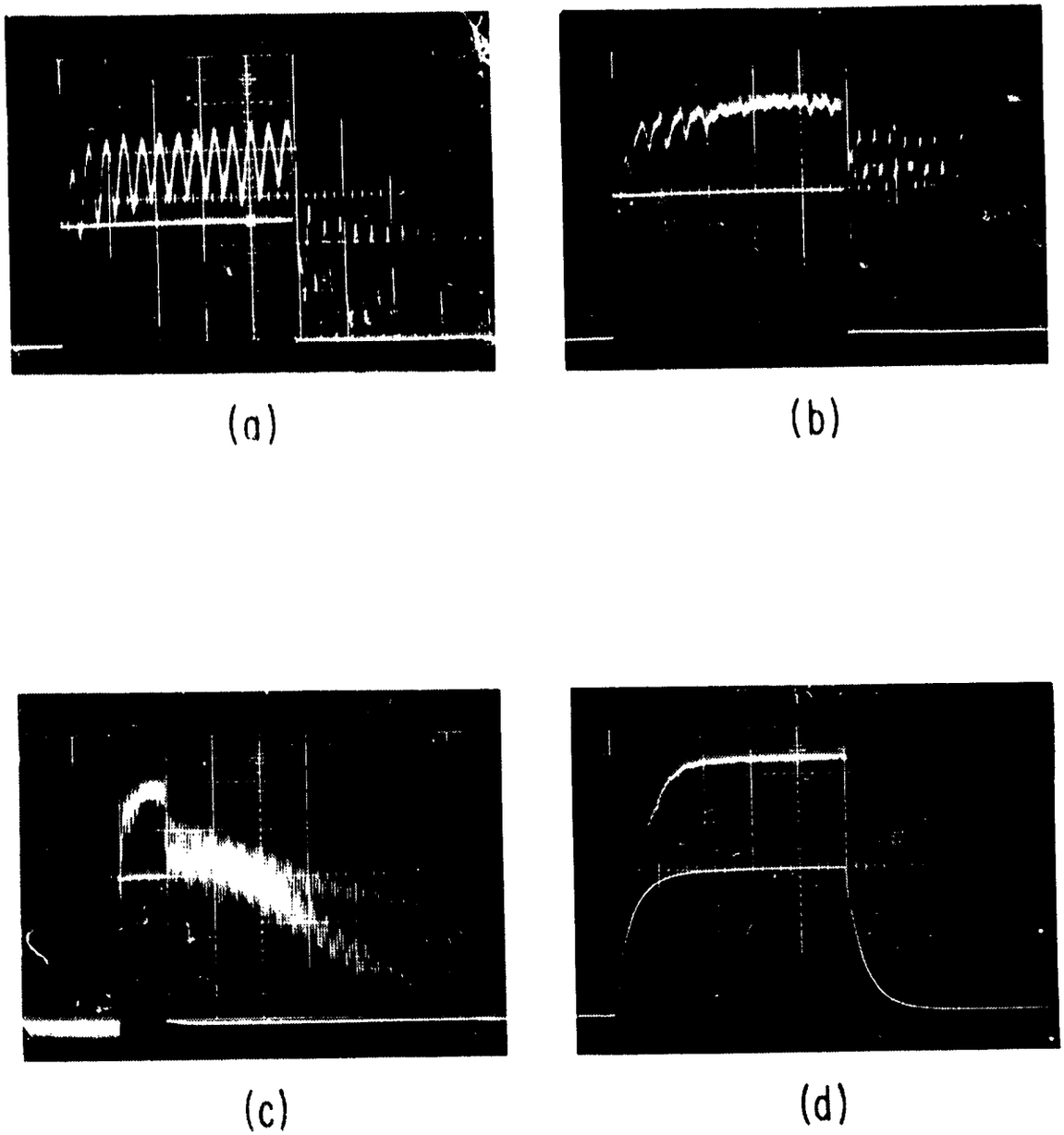

Figure 21. Pulse response in vacuum with changes in the applied voltage pulse amplitude and rise time for an element of line S1 on 2D-3. The voltage scale is 10 V/div. for all the photos. The time scale is 5 μsec/div. except for (c), where it is 25 μsec/div.
(a) Similar to Fig. 20(a) except that the voltage pulse amplitude has been increased.
(b) The voltage is increased further.
(c) Same as (b) but on a compressed time scale.
(d) The voltage pulse rise time has been increased resulting in reduced amplitude of oscillation.

which were made on ordinary glass with evaporated electrodes and connection pads on the same side of the substrate as the membrane. The use of feedthroughs introduced complications which did not exist for the elements previously described, and which affected operation of the circular elements. For example, the silver epoxy used as the feedthrough material is quite grainy and soft relative to the substrate. Consequently after the 0.25-mm-diameter holes were filled with the epoxy, and the substrate surface was ground and polished, the silver feedthrough surface was typically undercut and irregular. Therefore, if the feedthrough itself were used as the drive electrode, as it was in the earliest samples, it would be farther from the membrane than the support structure height, and non-uniform over its area as well as from element to element. Some improvement was obtained by evaporating 0.5-mm-diameter aluminum caps over and around the silver feedthroughs, and then grinding them back to get smoother, flatter electrode surfaces. This helped somewhat but the grinding operation again produced non-uniformities in electrode height, which caused corresponding variations in the voltages needed to deflect membrane elements a given amount. The next modification involved offsetting the feedthrough element from the optical element area, and insulating the feedthrough-electrode combination from the metal support structure with an SiO blanket. Thus, the drive electrode in the effective element area would be a deposited aluminum layer similar to that used for elements made on ordinary glass. Samples with plated-nickel membranes were made and tested with each of these types of electrodes used to drive the circular elements.

Circular elements were tested in the usual optical system to determine contrast and pulse response. Results for two samples are shown in Fig. 22. Maximum contrast is seen to be about 15 in the light intensity versus voltage curves. The pulse response of the two elements shown is seen to be rather slow. Again, it was found that switching time would vary markedly with the fastest times associated with elements having many holes in the membrane. One such response can be seen in Fig. 23, which shows light intensity versus voltage for the element as well as rise and fall times. One circular element of sample RX1 with a 0.6-μm-thick membrane was also tested in vacuum and found to resonate at 125 kHz when pulse-excited.

Experience with the 0.75-mm-diameter circular elements indicated that a device with a 0.8-μm-thick plated-nickel film for the membrane, and a separation of about 2 μm between electrode and membrane would meet our performance requirements.

D. NASA 8 × 8 Devices

Completed 8 × 8 arrays with individual access to each element were mounted on a holder and electrically connected to an electronics test panel, which could select and drive a single element or which could scan an array in a sequence determined by an external trigger. By viewing the image of the array on a screen, or letting it fall on a photodetector in the simulated optical memory system, operation of devices could be evaluated. More than half a dozen samples of this

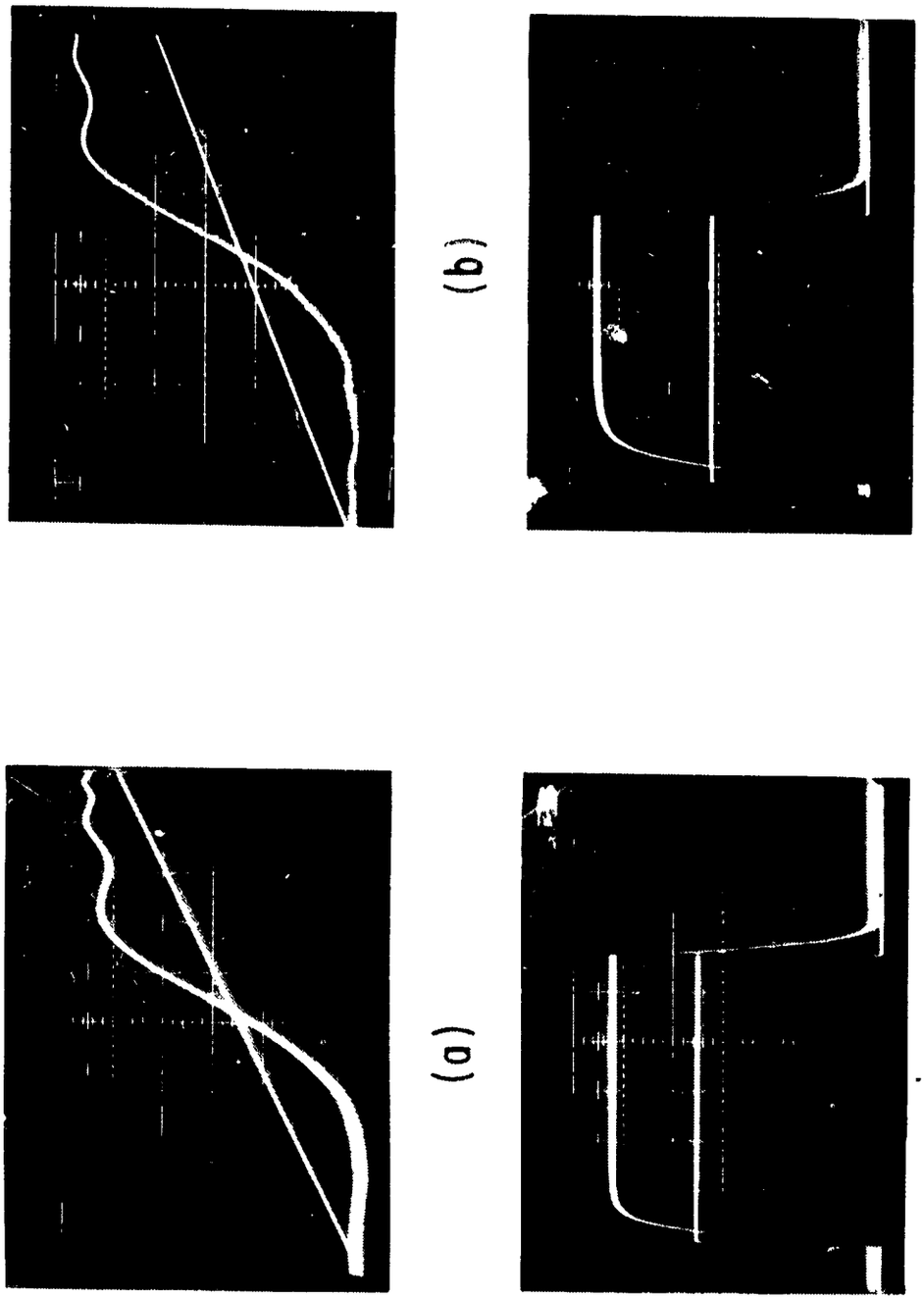

Figure 22. Detector output vs. applied voltage. The voltage scale is 10 V/div. for all photos.
(a) Element (5,5) of sample RX1.
(b) Element (4,5) of RC6.
(c) Pulse response of element (5,5) of RX1. The time scale is 0.5 msec/div.
(d) Pulse response of element (4,5) of RC6. The time scale is 1.0 msec/div.

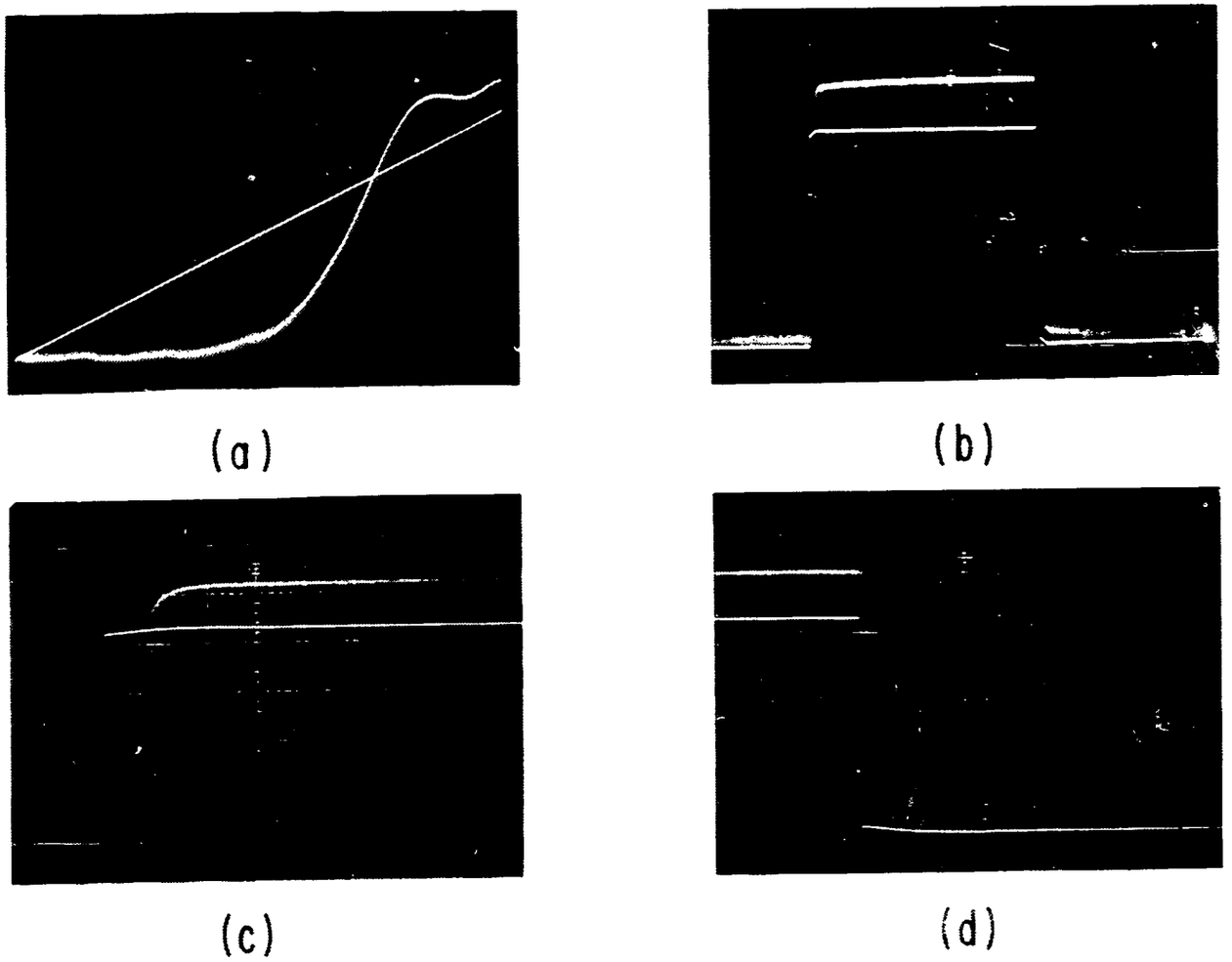

Figure 23. Detector output vs. applied voltage for element (1,1) of sample RC2. The voltage scale is 10 V/div. for all photos.
(a) Response to sawtooth voltage.
(b) Pulse response. The time scale is 100 μsec/div.
(c) Rise time of response. The time scale is 10 μsec/div.
(d) Fall time of response. The time scale is 10 μsec/div.

type were tested this way. Fast operation of an element was measured by driving it directly from a pulse generator rather than through the electronics control panel. The electronics are described more fully in Appendix A.

Some of the data obtained from 8 × 8 arrays have already been described in the section on circular elements. Other data involve uniformity over the array, and variation of properties with changes in dimensions or the geometry of the element. Using the control panel electronics an 8 × 8 array would be scanned at a low voltage, and the corresponding contrast of elements would be noted at the image of the array on a screen. As the voltage was increased in steps, further changes would be observed until the entire array was operating with good contrast or the reasons why it was not were determined. One common fabrication problem involved collapsed or partially collapsed elements on a completed sample. The first arrays were made using the feedthroughs directly as electrodes which resulted in many problems as previously described. The samples with 0.5-mm-diameter aluminum caps performed much better but were still non-uniform. The grinding step would leave the caps higher in the center of an electrode than at the periphery, and produce considerable variation in the height of an electrode from element to element on the same sample. One sample (RC6), with cap electrodes, when completed had all 64 elements intact, flat, and quite specular to the eye. However, two shorts between membrane and electrodes were found during electrical checkout. While other elements worked, they did not operate at the same applied voltage. Some elements had high contrast at 30-35 V, while others did not have good contrast until perhaps 45 V had been applied. Because the membrane on this sample was only 0.6-μm thick, it was not strong enough so that the cells which deformed at low voltage could withstand the higher voltages needed to operate other cells at high contrast. Consequently, several elements deformed permanently or tore when higher voltages were attempted. Operation at a "safe" voltage (~38 V) meant that some elements were not operating with a satisfactory contrast ratio. These problems were fairly typical of early samples.

Later samples with 0.75-mm elements were made with 0.8-μm-thick membranes, which proved to be more durable and stronger than the thinner ones. Other samples were made with the feedthroughs offset from the optical element area and the drive electrode beneath the entire 0.75-mm-diameter element. A blanket layer of silicon monoxide was used to insulate the feedthroughs from the aluminum support structure. Several shorts between the feedthroughs and supports were typically found on such samples even with SiO 2-μm thick. While we could make even thicker layers of SiO, we decided to try silicon monoxide support structures, thereby eliminating the need for aluminum supports and quite possibly easing the short situation. Early results with this technique have been encouraging and we will pursue it further.

Samples with multiple-element membrane light valves as described in Section VI have also been made on the Fotoceram substrates and tested in the usual way. Some of the same difficulties were encountered in making arrays of these elements as previously described for the circular elements.

Other tests made on NASA 8 × 8 devices involved simulations of the final device by connecting a MOSFET to an electrode of a sample, and evaluating the performance of the combination. Several semiconductor chips with four transistors on each, as designed and made by RCA Somerville, were cut, packaged in standard 14-lead DIP cases, and delivered to us. Tests showed that all of the original specifications had been met. The breakdown voltage between any two terminals of a MOSFET exceeded 50 V and in some cases was 70 V or more. In addition, pulse tests with simulated loads verified that the transistors could drive an element to 50 V in 1 μsec or less, with appropriate pulses on the gate (X) and data (Y) lines. Finally, the transistors on a chip were used to drive actual elements on a NASA 8 × 8 device by making the proper connections to the individual access pads. Some of the results are shown in Fig. 24 for element (3,3) of sample RC2, and a TC1022 experimental transistor driven with appropriate pulses. The top waveform is the data pulse (Y), the middle waveform is the gate pulse (X), and the bottom waveform is the light output from the detector. In (a), the gate pulse overlaps the data pulse completely, so that the element charges and discharges again when the data pulse occurs. In (b), the pulses are narrowed so that the gate width is 10 μsec. The storage effect is seen when the gate pulse terminates while the data pulse is still present. In (c), the pulses are narrowed further so that the gate width is about 1 μsec. Note that the contrast has decreased because the element did not charge fully in 1 μsec. In (d), the gate and data pulse amplitudes were increased to 40 V from 37 V. Note that full contrast is now obtained since the element does charge sufficiently in 1 μsec. In (e), the same waveforms are seen on an expanded time scale. These results are seen to verify proper operation of the transistor-light valve combination.

As a result of the preliminary tests with NASA 8 × 8 arrays, all phases of the delivery item fabrication and operation were evaluated, even before a device with all the components had been completed.

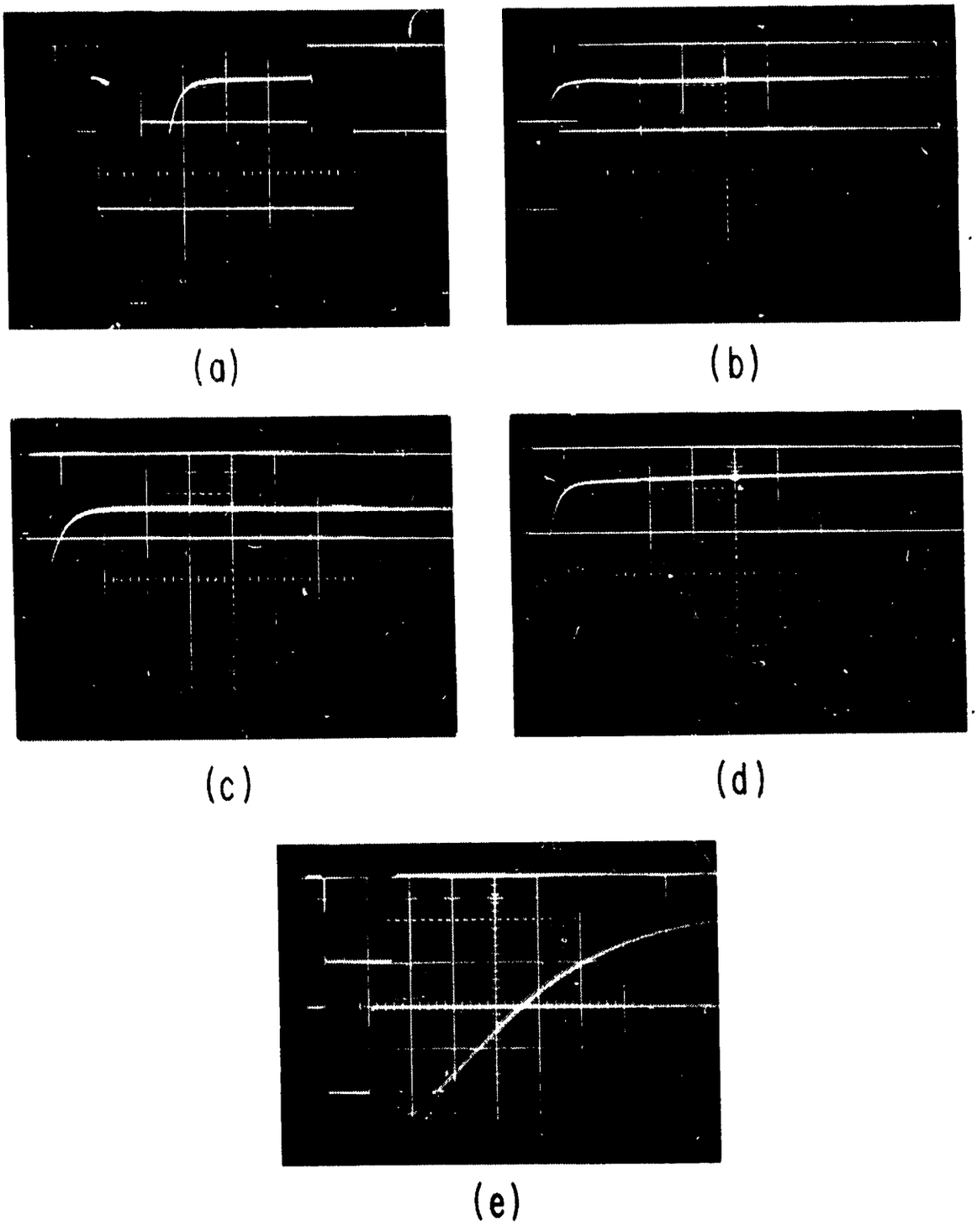

Figure 24. Waveforms showing simulated operation of the final device. The voltage scale is 20 V/div. for all the photos. The zero light level is at the top line of the graticule. The time scale is 10 μsec/div. for (a), (b), (c), and 1 μsec div. for (d).

VIII. DISCUSSION

It is of interest to consider the experimental data with reference to the analyses previously performed for electromechanical operation. Note that Eq. (5) predicts that the central deflection (z_o) of a line element with a constant built-in tension, is proportional to the square of the applied voltage (V), while Eq. (11) predicts that z_o of a line element with tension resulting only from elongation of the film is proportional to the two-thirds power of V. Figure 14 shows the experimentally found dependence of z_o on V. Figure 15 indicates two broad regions of exponential influence. For small deflections, the exponent of V (the slope of the lines through the points) appears to have a value of about 1.7-1.9, depending on how one draws a line through the points. For deflections larger than about 0.3 μm, the exponent is about 3.6. For the region of small deflections, we would expect that the built-in tension dominates since there is little elongation. Therefore, the exponent should be close to 2. As the deflections get larger, the assumption that $z_o << d$ no longer applies and one would expect that for fixed T_o, an incremental change of voltage would produce even greater deflection than predicted by Eq. (5), since the center of the element membrane is closer to the electrode than the nominal separation. This effect appears to completely override the effect of increasing tension caused by elongation. In fact, for deflections which are an appreciable fraction of the original separation, a runaway situation can and sometimes does eventually take place with the thin film collapsing on the electrode or tearing. The above data suggest that the built-in tension in the deposited film is much larger than that contributed by stretching of the film. The vacuum tests support this view because the resonant frequency of the membrane did not vary appreciably with changes in the amplitude of the exciting pulse. Another point in support of this view can be made by calculating the tension in a film from Eq. (13) repeated here for convenience

$$f_1 = \frac{1}{2W}\sqrt{\frac{T_o}{\delta t}} \quad .$$

For the line element of MC-7, for which the resonant frequency of 330 kHz was measured and for which W~.25 mm, $\delta \sim 2.7$ gm/cm^3, and t~0.6 μm, it turns out that T_o from the above equation is 44 Newtons per meter (N/m). This represents the total tension in the film regardless of the cause. Now we can estimate the component of tension in the film caused by elongation from Eq. (8), $T = (\Delta W/W)\,Et$. We have also previously calculated the incremental strain, $(\Delta W/W)$, for a deflection of 1 μm of a cell 0.25-mm wide and found it to be 0.43×10^{-4}. Using $E = 7.3 \times 10^{10}$ N/m^2 for aluminum-zinc in the equation, we can solve for the tension to find T~1.9 (N/m), which is less than 5% of the total tension in the film, even with a deflection of 1 μm. Thus, the tension introduced in the film during fabrication appears to be the dominant one. The total strain in the film would be about 0.1%, which is still small and well within the elastic limit of most metals. The experimental data support this point since no change in the operating

characteristics of an element was seen after 189 million cycles of excitation. It should also be noted here that in other work with membrane elements (ref. 1), no fatigue effects were seen even after 10^{12} cycles of operation.

The pulse response of membrane elements both in air and in vacuum showed that fast operation of these light valves is possible. In vacuum, vibrations at resonance must be avoided. This can be accomplished by using drive pulses having rise times which are slow relative to the natural vibration period of the element, but which can still be in the 5-10 μsec range. Another possibility is to bleed in enough air to critically damp the oscillations. In air, it was noted for both the square and the circular membrane elements that the speed of response is strongly affected by the number of micrometer-sized holes in the membrane. Fastest response (~ 10 μsec) was seen for elements with the most holes, which allow for the easy passage of air into and out of the membrane-to-electrode space.

The analyses of optical performance were very useful in understanding operation of the light valves, and in predicting experimental responses. The geometric optics approximation was useful in predicting that about 1-μm of deflection would result in an optical contrast of about 10 at the detector. This value in turn was used to calculate that about 50 V might be sufficient to operate a 0.25-mm-wide or larger element. The more complicated computer analysis which included considerations of diffraction effects also yielded useful results. One of these was the prediction of the oscillatory portion of the curve of the light intensity at the detector as a function of deflection, as can be seen in the calculated plot of Fig. 5, as well as in the numerous photos showing I versus V. The agreement between the calculated and observed behavior can be seen by comparing Fig. 5 with Fig. 16. The two plots are quite similar with the only appreciable discrepancy occurring in the location of the peaks and valleys of the oscillatory portion of the curves. The factors which may be contributing to these differences are the non-parabolic deformation of the element in the actual case, the differences in the reflectivity of the membrane and support structure, and the actual placement of components such as the focal plane aperture in the experiment. The qualitative analytical results concerning variations in illumination and in aperture size at the focal plane and/or at the detector have also been verified by experimental observations. It is clear that system trade-offs are possible to obtain high contrast operation of a MLV by the appropriate choice of aperture size used at the detector and in the Fourier transform plane.

Experience with the fabrication of light valves on ordinary glass substrates and on Fotoceram substrates with feedthroughs clearly pinpointed the problem areas which need to be worked on. Common to all the valves is the need for a defect-free membrane with no collapsed elements. Although difficult, this has been accomplished and can be done. In addition, the use of multiple-element valves alleviates the problem somewhat. More serious are the difficulties associated with the feedthroughs. Different materials should be investigated. Various improved techniques of filling and smoothing the etched holes for feedthroughs are possible, but have not yet been tried

because of time limitations. This type of problem is not fundamental and we believe it will yield to reasonable technological efforts to solve it.

Although the optimum technique for making an 8 × 8 array had not been developed we proceeded with the best of the available methods to fabricate the NASA delivery item. As of the writing of this report, RCA Somerville has several substrates with offset feedthroughs to which they are bonding the semiconductor chips. Most of them have an aluminum support structure while a few have SiO supports. After the chips are bonded and tested in place, we will finish the devices by adding a membrane. We will then evaluate the arrays and deliver them to NASA. Descriptions of all the preliminary tests which were already performed without the final device have already been given. In addition, we have ready a test holder and an electronics test panel to be used in evaluating the page composer. The electronics include an 8 × 8 semiconductor memory with LED indicators for storing and displaying a selected page composer pattern. Means are provided to address an element in various modes. Drive pulse duration and repetition rate are variable over wide ranges. Data can be entered at TTL levels either manually or electronically. Further details are found in Appendix B.

IX. CONCLUSIONS

The feasibility of producing a membrane light valve page composer for optical memory systems has been demonstrated. Membrane light valves located over a 1/2-inch square area were operated at high speed with good contrast, efficient utilization of light, and without fatigue. The electromechanical and optical performance of membrane elements have been analyzed and agree well enough with experimental results to give confidence in the models. It is now clear that membrane elements make excellent light valves. What remains to be shown is that arrays of such valves can be produced without serious defects, and with enough uniformity to operate within practical tolerances.

Arrays of 64 individually accessible elements have been made on substrates with feedthroughs and tested. Single elements of the arrays have been successfully operated with the MOS transistors designed and produced for selection and storage of a bit. In this way simulation of the operation of elements with semiconductor chips bonded to the substrate was accomplished. All of the preliminary tests have been completed and fabrication details have all been worked out. All that remains is evaluation of the final device when it is completed.

While no perfect 8 × 8 arrays were produced, it should be pointed out that a prototype was the goal with no optimization claimed for any of the fabrication steps. All of the remaining problems appear to be small ones which should yield to technological effort. Many ideas for improvements generated during the project were not pursued for lack of time. The next phase of the work should incorporate these improvements as well as extend the active area and capacity to include a larger array such as a 16 × 16.

APPENDIX A

Electronics I

The photograph of Fig. 25 shows the front panel of the electronic equipment used to test the 64-element individually accessible membrane light valve samples. It is used with a variable positive-voltage power source which controls the voltage applied to the membrane elements. To use the cycle address mode it is also necessary to connect an external pulse generator. The function the machine performs is to address one of the 64 elements and apply the test voltage to it.

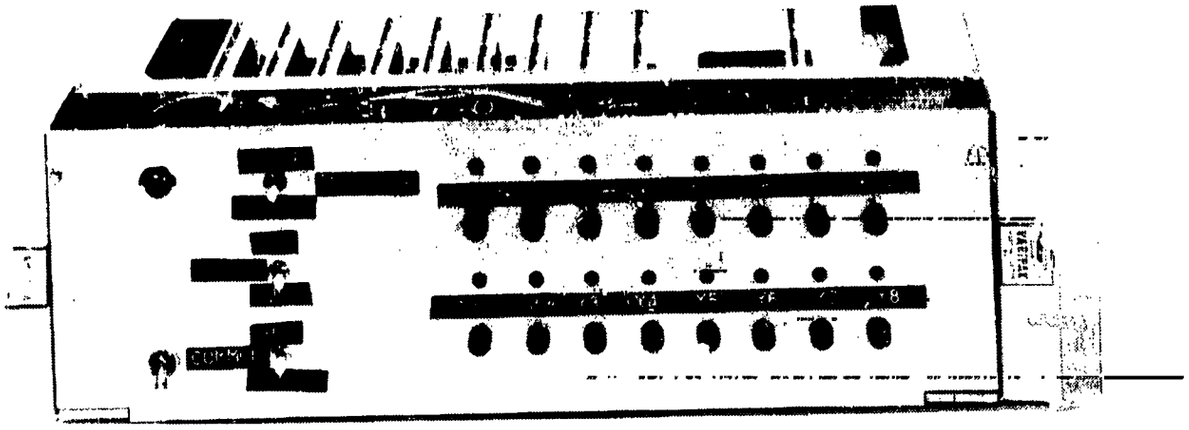

Figure 25. Electronics I test panel.

Figure 26 is a block diagram illustrating operation. Addressing of an element is accomplished by operating one of the 8X switches and one of 8Y switches. Operation of any of the 16 address switches initially resets the appropriate register (X or Y). Simultaneously it is encoded into a 3-bit binary word and stored in the register. The two 3-bit address numbers are used as inputs of a 64-wire decoder. The decoder, in turn, drives 64 voltage switches of the type shown in Fig. 27. The outputs of the 64 switches are connected to the feedthroughs of the array.

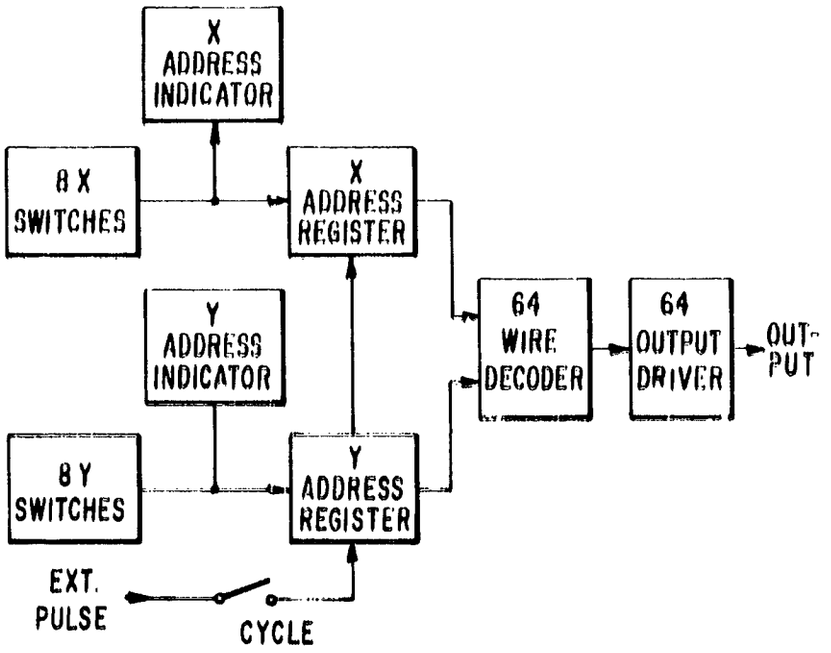

Figure 26. Block diagram of Electronics I test panel.

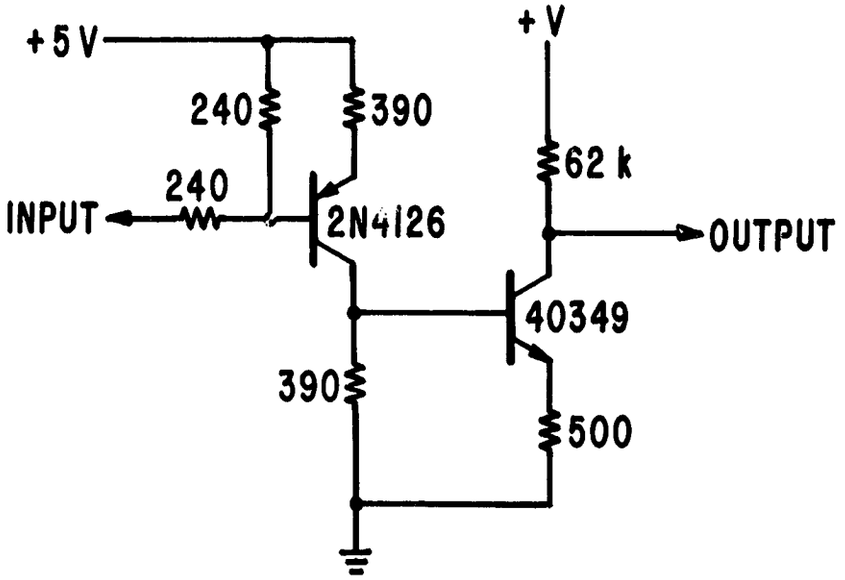

Figure 27. Circuit of output driver.

Cyclic operation is obtained by connecting the external pulse generator to the pulse input and setting the ADDRESS switch to cycle. This reconnects the registers as counters operating at a rate determined by the external pulse generator.

The output stage is shown in Fig. 27. The input operates at logic levels. The output is capable of 100 V pulses. Output currents are limited to less than 2 mA to both ground and the positive-voltage power supply. Circuit speeds are limited by the load resistors and cable capacitance to the light valve, on the order of 100 μsec.

APPENDIX B

Electronics II

Electronic control of the NASA 8 × 8 page composer array is achieved by a machine which provides all the signals needed to test the page composer. It has the additional capability of operating in a larger system. This is accomplished through the use of a 64-bit buffer memory. The buffer is loaded from either front-panel switches or an external source through a rear-panel connector. With the exception of the output drivers, the design was performed using TTL logic circuits.

A photograph of the front panel is shown in Fig. 28. The controls and indicators are arranged in three groups of related functions.

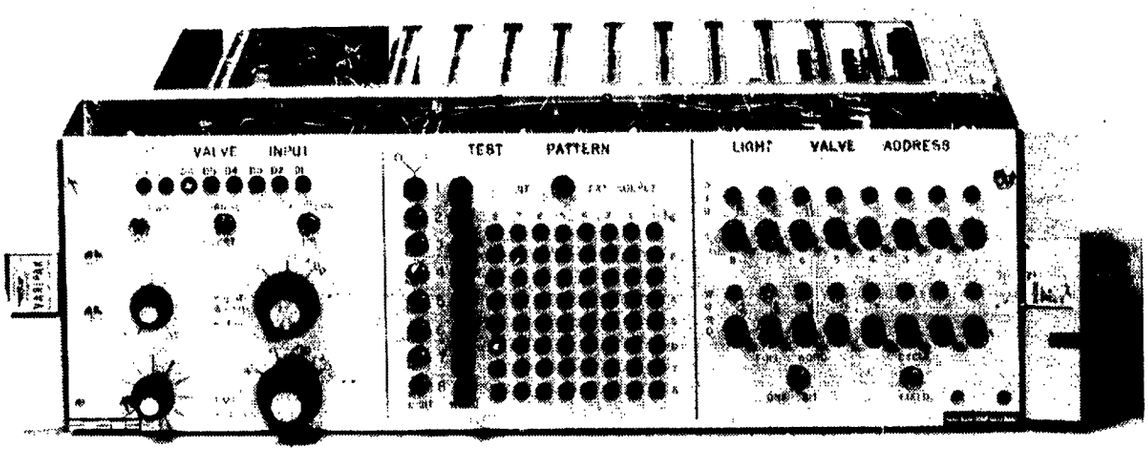

Figure 28. Electronics II test panel.

First are those which perform word and digit addressing of the light valves and simultaneously the output of the buffer memory. Several modes of addressing are provided.

The test pattern section of the panel contains an array of 64 LED'S indicating the state of the buffer memory. A toggle switch selects the source of signals which construct the pattern. This is either the double column of switches or the rear panel connector.

The last grouping contains those controls which are more directly concerned with inputs delivered to the light valve. These include such things as cycle time, pulse duration, the "polarity" of the pattern, etc.

Several conventions were adopted during the circuit design. The array of 64 LED's has been wired and labled such that the contents of word 1 are indicated by the top row of LED's and word 8 by the bottom row of LED's. Additionally, the least significant bit of each word (D1) occupies the right-hand column and the most significant bit the left-hand column. The storage of a "1" in the buffer memory lights a LED. The circuit design is such that when a "1" is stored in the buffer and a LED is lit, the corresponding element of the page composer will be reflecting light specularly. There is a direct relationship between the position of any LED within the array and its related element within the array of light valves. The NORMAL/INVERT switch provides the means for complementing the pattern at the input of the page composer. This results in dark spots in the image where bright spots are indicated by the pattern generator.

The address and digit lines are pulsed under control of an internal oscillator and pulse generator. The oscillator's first panel controls are labeled CYCLE TIME which is continuously variable from 20 μsec to 0.2 μsec. The cycle time is the interval between successive addressing pulses to any individual element of the page composer. The first panel calibratior is true for all but one setting of the mode switches. The address pulse width is variable from 0.5 μsec to 500 μsec.

The equipment is designed to operate at a fixed word address or cycle sequentially through all addresses. Through the use of the ONE BIT setting (FULL WORD/ONE BIT switch) a quasi-bit mode of addressing is possible. The addressed bit (as indicated by the word and digit address indicators) operates normally. The other 7 bits of the addressed word are driven dark if the NORMAL/INVERT switch is set to NORMAL, and bright if it is set to INVERT. With the switches set to ONE BIT and CYCLE the ambiguity in the definition of cycle time arises. Under these conditions the bit address is changing at the indicated rate.

The eight indicators labeled D1 through D8 show the state of the input lines to the page composer. They all agree with the image of a word after it has been loaded.

The block diagram of Fig. 29 shows the address generator. Word address numbers (and bit address numbers when required) are internally represented by a 3-bit binary word. Depending on the state of the CYCLE/FIXED mode switches these are generated or stored in a 3-bit binary counter/register. With the switch in the FIXED position carry pulses into the word counter/register (and the bit counter) are disabled and the contents are stored indefinitely. The state of the register is indicated by the appropriate word indicator. A new address can be selected by pushing the desired word switch. This contact closure is translated into a 3-bit binary code and simultaneously a timing sequence is initiated whereby the register is cleared and the new code is stored. The output of the register is decoded back to decimal for control purposes and to drive the front panel word address indicators. The 3-bit word number is delivered to the buffer memory within the pattern generator and the word drivers of the light valve input circuits.

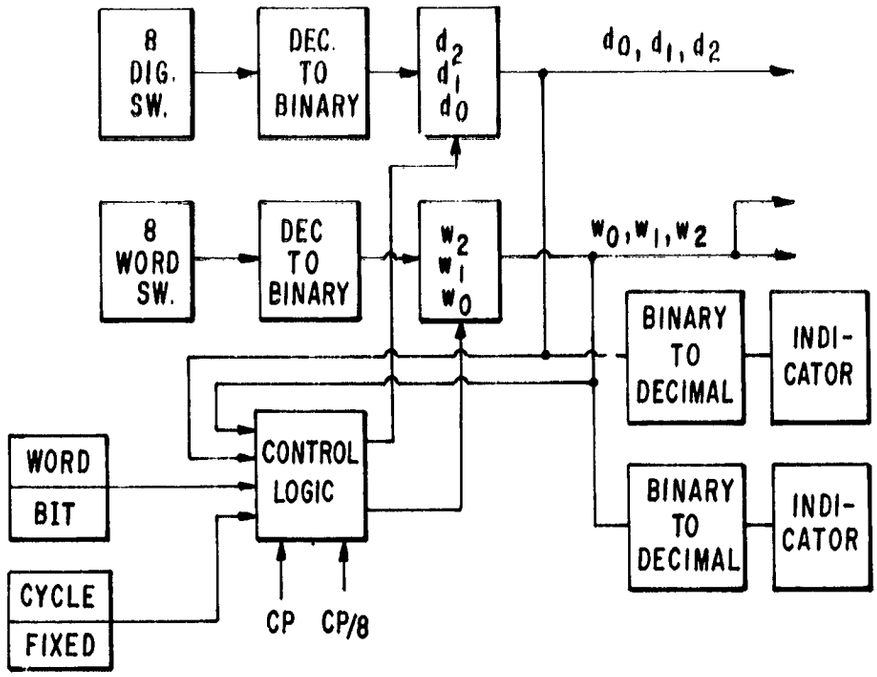

Figure 29. Block diagram of light valve address generator.

When the FULL WORD/ONE BIT switch is operated in the ONE BIT position, the bit address circuits operate in much the same way as the word circuits. The 3-bit digit-address number is delivered to light valve input circuits. As with the word circuits, the digit-address number is decimal decoded at the address circuit for control purposes and to drive the front-panel digit-address indicators.

With the switch operated in the FULL WORD position, the digit-address generator circuits are disabled and the digit address indicators are all lighted. A complete 8-bit data word is delivered to the page composer.

Cyclic operation through all addresses is obtained by operating the CYCLE/FIXED switch to CYCLE. If the FULL WORD mode of operation is used, the digit-address generator remains inhibited.

With the switches operated to ONE BIT and CYCLE both counters are operating and input carries are derived from CP/8. Whether a carry or borrow input is delivered to the digit counter depends upon the sense of the word number. Odd word numbers drive the digit address up from 1 to 8. Even word numbers drive it back from 8 to 1. Carries into the word counter are generated

when the digit address is either D1 or D8. This connection makes the addressed active bit propagate through the array in a serpentine fashion from W1D1 to W1D8 to W2D8 etc.

Figure 30 is a block diagram of the pattern generator. The main element of the pattern generator is a 64-bit word-organized memory. The state of each storage location is indicated by a LED on the front panel. Depending on the position of the INT/EXT SOURCE switch, the memory is loaded from the panel switches or the rear connector. The memory is loaded a word at a time by setting the digit switches and then processing the appropriate word switch.

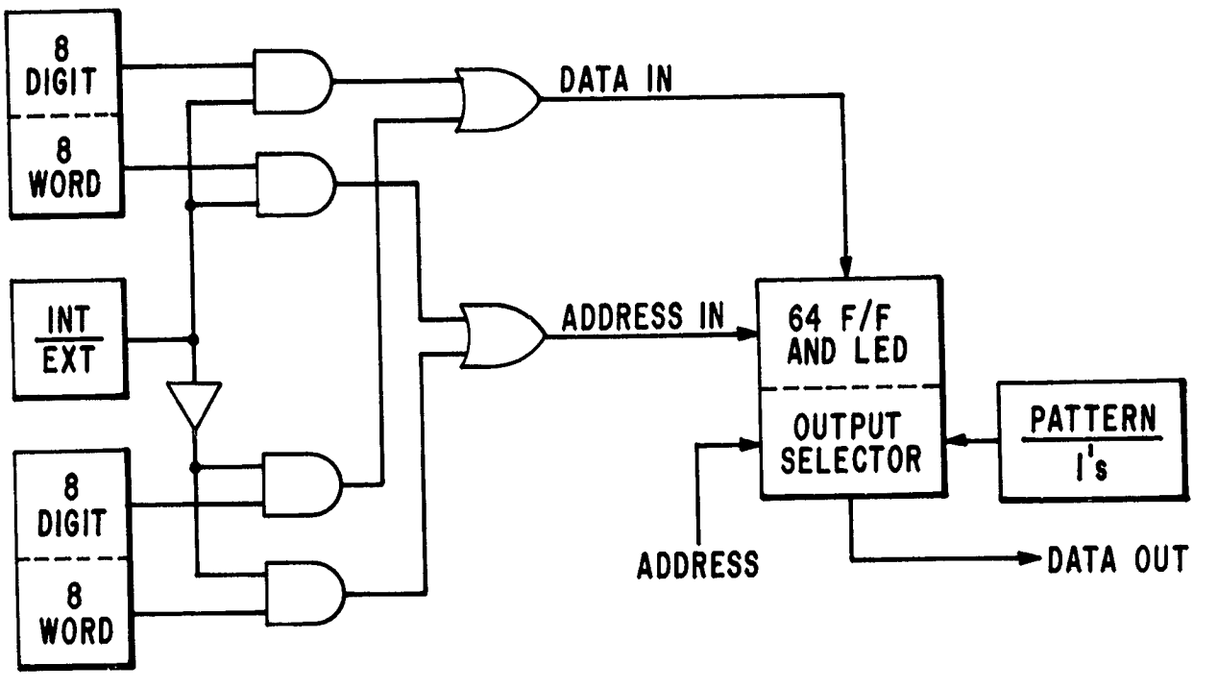

Figure 30. Block diagram of pattern generator.

The memory output circuits are under control of the light valve address circuits; input and output are independent. The 3-bit word number generated by address circuits accesses the appropriate 8-bit word and delivers it to the drivers.

Although located within the LIGHT VALVE INPUT section of the panel, the PATTERN/1's switch was most easily mechanized within the memory. When set to the 1's position it inhibits the memory-output circuits. This produces an effect on the following circuits as if the memory was loaded with 1's.

The remaining input circuits are illustrated in the block diagram of Fig. 31. The oscillator and its related divider and pulse forming circuits control the system timing through the word and

digit enable pulses and the input carries to the address generator. This is accomplished by generating two similar pulses, CP and CP/8. The setting of the mode switch determines which is used. For example, with the switches set to WORD and CYCLE the logic is such that the enable pulses are generated every CP time and the word address changes at this rate. The individual elements pulse at a rate of CP/8 as a result of the changing address. With the switch set to FIXED, the pulse CP/8 is used to initiate the enable pulses.

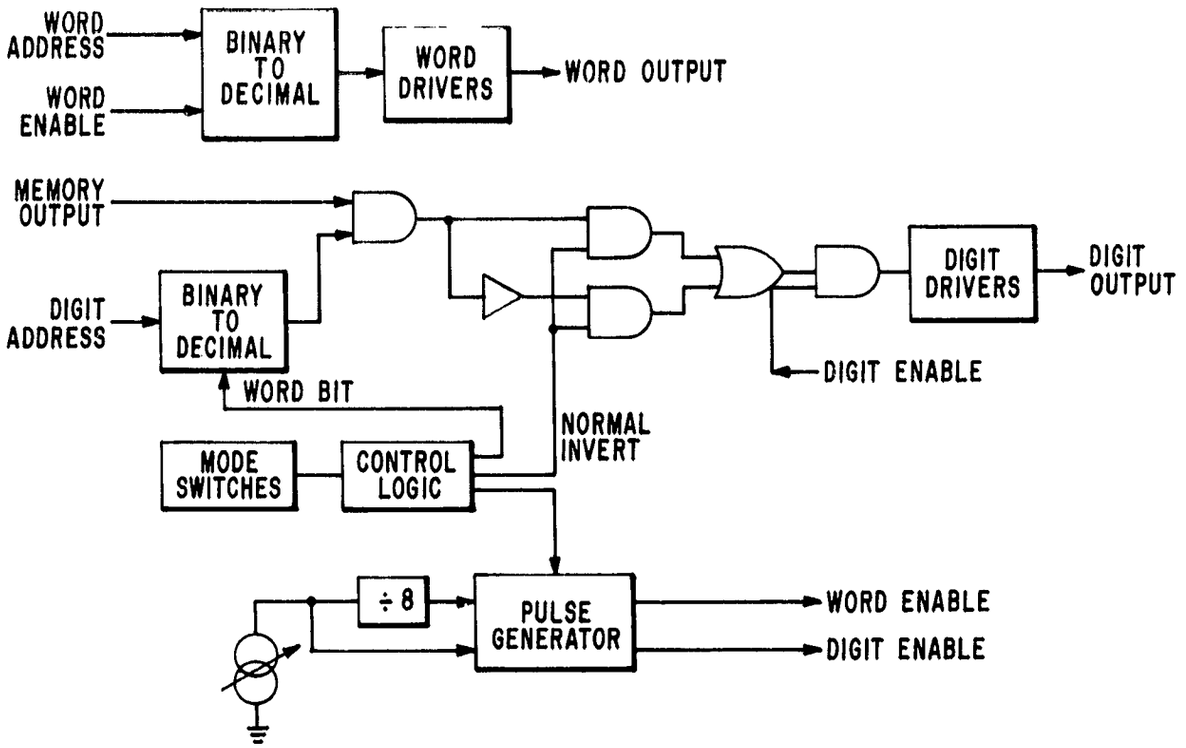

Figure 31. Block diagram of light-valve input circuits.

The word-enable pulse is derived from a variable-width pulse generator. The trailing edge starts a 0.2 μsec pulse which is added to the original pulse to form the digit-enable pulse. This insures that the light valve elements remain in their driven state as the pulses are removed.

The 3-bit word number is combined with the word-enable pulse in a binary-to-decimal converter. This results in one wire of eight pulsing at the correct time. These outputs drive the word-line drivers one of which is shown in Fig. 32. The digit lines are driven by similar circuits. Connection is made to the light valve array through a cable which is over 10 feet long. The cable contains 16 pairs plus eight additional shield leads. This results in circuit capacitance of 25 pF per foot. The word and digit drivers deliver pulses at the array end of the cable with rise and fall times of 0.1 μsec and 0.3 μsec, respectively.

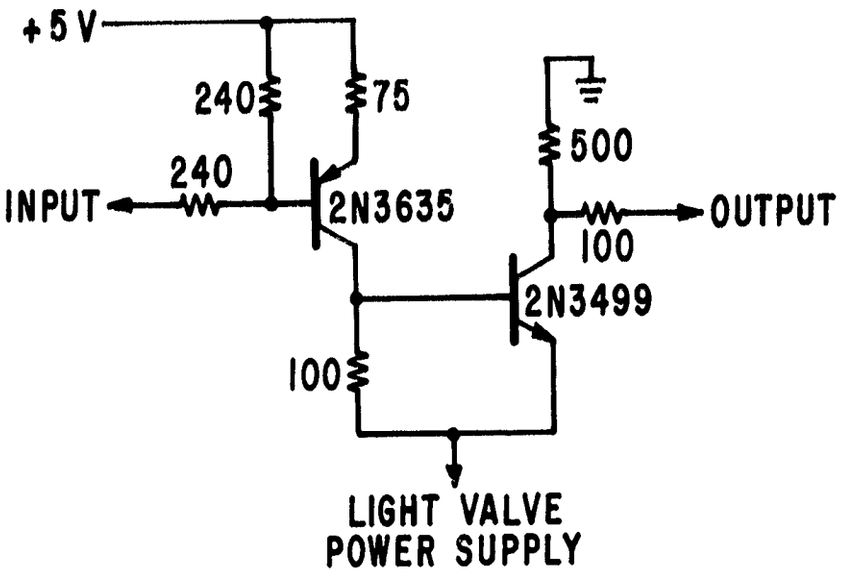

Figure 32. Circuit of output driver.

Digit information received from the pattern generator is modified, or not, according to the setting of several switches. The LED's indicate the state of the inputs to the digit-line drivers. The NORMAL/INVERT switch inverts the sense of the pattern. For example, with the switches set to NORMAL and 1's, all elements are bright. With the switches set to INVERT and 1's, all elements are dark.

The L.V.PWR/OFF switch applies voltage to the word and digit drivers. This is derived from an external power supply connected to a rear-panel connector. This voltage should be negative only and limited to a maximum of 50 V.

REFERENCES

1. K. Preston, Jr., "A Coherent Optical Computer System using the Membrane Light Modulator" Trans. IEEE, Aerospace and Electronic Sys., AES-6, 458 (1970).

2. F. Reizman, "An Optical Spatial Phase Modulator Array, Activated by Optical Signals" Proc. Electro-Optical Systems Design Conference, 225 (1969).

3. J. A. vanRaalte, "A New Schlieren Light Valve for Television Projection", Appl. Opt. 9, 2225 (1970).

4. S. Timoshenko, *Theory of Elasticity* (McGraw-Hill Book Co., New York, 1934) p. 245.